Methods of Optimal Control for Fuel Efficient Class-8 Vehicle Platoons Over Uneven Terrain

by

Jacob Ward

A thesis submitted to the Graduate Faculty of
Auburn University
in partial fulfillment of the
requirements for the Degree of
Master of Science

Auburn, Alabama
August 6, 2022

Keywords: model, predictive control, platooning

Approved by

David Bevly, Bill and Lana McNair Professor
Scott Martin, Professor of Mechanical Engineering
Mark Hoffman, Professor of Mechanical Engineering
John Hung, Professor of Electrical and Computer Engineering

Abstract

This thesis implements an NMPC control system to facilitate fuel-optimal platooning of class-8 vehicles over challenging terrain. Prior research has shown that Cooperative Adaptive Cruise Control (CACC), which allows multiple class 8 vehicles to follow in close proximity, can save between 3-8% in overall fuel consumption on flat terrain. However, on more challenging terrain, e.g. rolling hills, platooning vehicles can experience diminished fuel savings, and, in some cases, an increase in fuel consumption relative to individual vehicle operation. This research explores the use of Nonlinear Model Predictive Control (NMPC) with pre-defined route grade profiles to allow platooning vehicles to generate an optimal velocity trajectory with respect to fuel-consumption. In order to successfully implement the NMPC system, a model relating vehicle-velocity to fuel-consumption was generated and validated using experimental data. Additionally, the pre-defined route grade profiles were created by differencing a vehicles GPS-velocity over the desired terrain profile. The real-time NMPC system was then implemented on a two-truck platoon operating over challenging terrain, with a reference vehicle running individually. The results from NMPC platooning are compared against classical proportional-integral-derivative (PID) platooning methods to obtain comparative fuel-savings and energy efficiency. In the final analysis, significant fuel savings of greater than 14&20% were seen for the lead and following vehicles relative to their respective traditional cruise-control and platooning architectures.

Acknowledgments

I would like to begin this thesis by extending a special thank you to my family. Every member played an important role in helping me maintain my sanity during the heavy months of work that went into the making of this thesis. To my parents, thank you for instilling in me a strong work ethic and dedication to excellence. Your constant support and encouragement to go the extra mile made a world of difference in the final months of this work. To my brother Sam and sister-in-law Jess, thank you for keeping an open door for me down in Florida, the weekend escapes went a long way to helping keep things in perspective. To my sister Susie, thank you for your willingness to listen to all my complaining and willingness to provide encouragement when I felt like there was simply too much left to be done. Without my family, this work would not have been possible.

I must also thank my advisor Dr. Bevly for providing an excellent place to work. My time in the GAVLAB was exciting and dynamic. Being able to travel the country and attend multiple conference and even present at a few went a long way to helping me understand the role my work was playing within the controls community. I appreciate the confidence you placed in me to help lead several of these trucking projects to fruition.

I would be remiss if i didn't recognize several members of the Siberia office. To Patrick Smith and Robert Brothers, thank you for your no-holds-barred critiques of my early work in the lab. Through a little tough love and a steep learning curve I was much better set up to tackle the challenges of leading solo projects that are sustainable later on. To other GAVLAB members, Brendan, Will, Matt, Anderson and more, i appreciate your friendship, brainstorming sessions and trips to the local "cafe" on Friday nights.

Additionally I must thank some core members of the truck team both past and present. Patrick Smith, Dan Pierce and Evan Stegner. Thank you for being an absolute pleasure

to work with. The late nights, early mornings and last second mechanical failures really forges a certain bond in the team that has to endure it. I couldn't have asked for a better group to take on these challenges. During COVID times the deadlines and challenges only got tougher to conquer. Thank you Evan for the positive attitude and willingness to work through anything during the months of COVID. This project would not have succeeded without your help!

Last but certainly not least i would like to thank God for blessing me with the ability to work on these projects. This journey was long and unexpected. There were more twists and turns in the process of writing than I would have ever thought. I would not have been able to finish this thesis without His grace and peace.

Table of Contents

List of Figures

List of Tables

List of Abbreviations

ECEF	Earth-Centered-Earth-Fixed
ELD	Electronic Logging Devices
ENU	East,North,UP
HoS	Hours of Service
INS	Inertial Navigation system
MPC	Model Predictive Control
NCAT	National Center for Asphalt Technologies
NMPC	Non-linear Model Predictive Control
SNR	Signal-to-Noise ratio
TDCP	Time-Differenced Carrier Phase

Chapter 1

Introduction

1.1 Background and Motivation

Trucks in the class-8 category travel approximately six times as many miles as passenger vehicles [1]. The average marginal operating cost of fuel on a fleet owner is approximately 24%, due in part to the relative inefficiency of these vehicles [2]. As a result, fuel savings technologies have become a major area of research on class-8 trucks as even small average fuel savings will save companies a substantial amount of money annually.

There are three main types of fuel-savings technologies that have been investigated for class-8 vehicles: device, vehicle, and driveline. Device technologies are typically passive and can be added to existing fleet vehicles. Examples of these would be trailer side-skirts and boat tails added to the rear of a trailer to help reduce aerodynamic losses. Vehicle technologies are usually more active in how they increase fuel economy. Two examples are cruise-control, which maintains a constant speed and speed governing, which limits vehicles to more fuel-optimal speeds. Driveline technologies can also fall under the passive subcategory and mainly pertain to things such as friction, wear and lubrication. However there is a category of active driveline technologies which includes the automatic-manual transmission.

The research in this thesis focuses mainly on the vehicle category of active fuel-savings technologies. When multiple vehicles follow in close proximity they are called a platoon. Sharing of information between platooning vehicles creates a technology called Cooperative Adaptive Cruise Control (CACC). CACC platooning technology has the capability of reducing fuel consumption of platooning vehicles by an average of 7% [3]. The following sections

will discuss the current state of the art methods for achieving optimal platooning performance, detail the contributions of this thesis, and provide a brief outline for the rest of the thesis.

1.2 Prior Research

Platooning is not a recent technological advancement. However, the motivations and technical challenges with platooning have changed over the years. Some early works in platooning can be seen through the 90's with some of the most relevant and cited work in platooning coming around 2000 [4]. The work from [4] dealt with passenger cars and was more motivated by increasing highway safety and highway capacity rather than fuel benefits. This thesis also introduces a common definition and synthesis methodology for string stable controllers. This methodology creates a linearized aggregate state matrix that includes the dynamics of every vehicle in the platoon. This aggregate state matrix is then subjected to certain spectral constraints that will generate control gains that yield a string stable platoon. String stability in this case is defined as disturbances diminishing for every vehicle in the platoon. This concept will be further explored in later sections. The concepts developed in [4] can be seen as the core emphasis for even more modern platooning works [5–7].

More recently, companies have also started investigating the use of platooning technologies. Some early work on Class-8 vehicle platoons with an emphasis on fuel efficiency begin to emerge around 2013 when Peloton presented fuel results from a 2-truck platoon following the J1321 fuel test standard [8]. Other companies and research institutions followed shortly to begin investigating the aerodynamic benefits of platooning [3, 9–11].

Among the works cited this far one should note that the primary controller design methodology is a classical controls approach. Classical controls in this context include all variations of proportional-integral-derivative (PID) controllers as well as H_∞ controllers. It is important here to lump H_∞ controls in with classical controls since the physical implementation of this control type usually follows state feedback or a PID scheme.

Classical control schemes work well for passenger vehicles which have larger power-to-weight ratios than loaded class-8 vehicles. Class-8 vehicles suffer from lower power-to-weight ratios and also have a more limited operating engine RPM band which results in more frequent shifting. The result of these differences means that class-8 vehicles will frequently run into actuator saturation issues as well as dead-time delays when shifting from gear-to-gear. While some works try to incorporate delays in some aspects of their controller development this only includes constant delays and does not include periodic delays such as gear shifts [12]. More recently however, cooperative shifting techniques have been investigated, showing a substantial fuel benefit for the platoon [13].

Furthermore, with a limited power-to-weight ratio these class-8 vehicles can often run into actuator saturation problems. A reader knowledgeable in controls may think that implementing a simple anti-windup scheme could easily mitigate this issue, however it is not quite so simple. First, many vehicle cruise-controllers use a PD architecture with no integral-control, which would make an integral anti-windup scheme pointless. Largely the saturation problem lies with the fact that with small changes in grade, a class-8 vehicle may not be able to produce enough power to maintain a constant speed. This effect is further complicated because in order to produce more power, a class-8 vehicle will shift down a gear, introducing the dead-time delay.

These combined effects of dead-time delays and actuator saturation are of extreme importance because they are frequent occurrences in actual platooning applications and they both violate some implicit assumptions made in the classical controls design methodology. Because the delays and saturation affects are violated, guarantees on platoon string-stability can no longer be relied upon.

With the shortcomings of these classical control approaches on class-8 vehicles, it is not surprising that some of the most promising and prominent works for practical platooning utilize non-linear model predictive control (NMPC). In 2010, Wei huang proposed a method of using NMPC to achieve fuel-optimal cruise control over terrain for a single class-8 vehicle

[14]. His work introduced a method for relating wheel-speeds to the vehicle's fuel rate through a "3-link" relationship. This relationship is commonly used in many other works such as [15, 16]. The work by Turri and Alam additionally relied on pre-defined terrain maps to allow for grade information to be taken into account during the optimization process. For a single vehicle, this optimal velocity approach was able to achieve savings of approximately 3%.

The approach taken by [14] was then adapted to a multi-vehicle platoon [15, 16]. In [15], Alam presented several approaches to the fuel-optimal problem by introducing Look Ahead Control (LAC), Adaptive Look Ahead Control (ALAC) and Cooperative Look Ahead Control (CLAC). While each of these strategies differ slightly in terms of their implementation, the underlying concept remains constant. The LAC concept uses the upcoming grade profile, and optimizes the vehicle's velocity profile using the 3-link relationship while maintaining some nominal following distance from the leading vehicle. ALAC relies on Vehicle-to-Vehicle (V2V) communication to have a leading vehicle share its optimal velocity profile with a following vehicle. The following vehicle can then optimize its velocity profile to mitigate any chance of a collision. CLAC selects a common platooning strategy from LAC/ALAC and imposes the common strategy across all platooning vehicles such that an overall platooning objective may be achieved. The Fuel testing in this thesis saw benefits of up to 14% fuel savings were possible when implementing the CLAC strategy over rolling hills.

One of the most recent and state of the art papers is [16], which again adapts the 3-link methodology to relate wheel speed to fuel-rate. The main contributions are the inclusion of aerodynamic effects into the system model and the introduction of a novel control architecture. Including the effects of air-drag reduction is an important inclusion because it allows for a more accurate model of inter-vehicle spacing dynamics. By noting the reduced air-drag on following vehicles, the optimal control will require less engine torque to maintain speed and can allow coasting on downhill segments since the follower will accelerate more quickly down hills.

LAC methodologies tend to look distances greater than a kilometer ahead in order to fully capture hills withing their scope. Due to the curse of dimensionality, this can cause large enough optimization computation times that real-time control would not be possible. Depending on the size of the problem, optimizing in real time even without including safety constraints may not be possible. To prevent this issue, the authors in [16] introduced a two layer controller approach. There is an overarching "platoon coordinator" that generates a common velocity profile to minimize fuel that every vehicle in the platoon is expected to follow. This adapts the CLAC philosophy and eases some of the optimization burden for the individual trucks in the platoon. Once every truck in the platoon receives an optimal velocity profile form the platoon coordinator, a lower level optimization occurs that uses a linear vehicle model to minimize the velocity error to the generated reference path. Additionally, the lower level controller receives information from other vehicles in the platoon and is able to include safety constraints to mitigate the possibility of a collision among vehicles in the platoon. Using this two-level control approach the following vehicle reported up to 12% better fuel economy versus traditional platooning controllers.

1.3 Contributions

While previous works have designed and in some cases tested optimal platooning controllers, none of the previous works using NMPC have done strict J1320 type-2 fuel testing. This is a major gap because day-to-day or even hour-to-hour weather and wind variations can cause sizable discrepancies in fuel consumption. Additionally, while CLAC is extremely beneficial in reducing the computation time and computational complexity, it is not always feasible or realistic to assume that platooning vehicles will be of the same brand or have a standard interface. Additionally in the case of a non-homogeneous platoon, it is also unrealistic that a "platoon coordinator" would have knowledge of vehicle parameters for every vehicle in the platoon. Therefore the contributions of this thesis are as follows:

- Develop a distributed NMPC approach to allow for non-homogeneous platooning

- Conduct fuel testing in the spirit of the SAE J1321 type-2 fuel testing standard
- Test various configuration of classical/optimally-controlled two and four truck platoons over several types of terrain
- Analyze fuel savings results and general trends

1.4 Thesis Outline

The rest of this thesis has 7 remaining chapters. Chapter 2 covers the derivation of the longitudinal equation-of-motion for the class-8 vehicle and a method of relating a vehicle's wheel speed to fuel-rate, which will be the backbone of the optimization process. Chapter 3 covers an easy and real-world tractable method of building a database of road-maps that relate grade to position. Chapter 4 covers the original method of platooning and its shortcomings on adverse terrain, and also introduces a method of classical control design to try and resolve those shortcomings. Chapter 5 then introduces the new method of optimal control for both the leading and following vehicles. Chapter 6 covers the simulation results from the controllers developed in chapter 5. Chapter 7 presents both the experimental testing design and analysis method. Then, experimental results are presented and the fuel-savings trends are analyzed. Finally, Chapter 8 will provide a high level overview of the full thesis reiterating many of the key chapter highlights through the thesis, and present some areas of improvement for future work.

Chapter 2

Platooning Vehicle Overview

This chapter aims to introduce the equations that govern the longitudinal motion of a class-8 vehicle as well as the hardware and software components that enable autonomy on the platform. Figure 2.1 displays the class-8 vehicles used as the platooning vehicles in this work. There are a four test vehicles in total. Two are Peterbilt 579's, and two are Freightliner M915's. One of the M915's is an armored variant (left) with substantially more weight than the other which is an unarmored variant (right).

Figure 2.1: Auburn Research Vehicles Used for Testing

Table 2.1: Specifications for the Trucks Used in the Thesis

Model	Mass [kg]	Power [kW]	Transmission
2009 M915A5	22888	322	Allison 4500 6 Sp
2009 M915A5	19513	322	Allison 4500 6 Sp
2015 Peterbilt 579	32000	322	Eaton Fuller 10 Sp

Through the introduction of various system models, a "3-link" fuel-rate model can be developed. This 3-link mechanism relies on estimating vehicle engine speed, engine torque,

and then fuel-rate. The following sections will introduce each method individually and conclude with an experimental validation of the fuel-rate model which demonstrates a mean fuel-consumption error of under 1%.

2.1 Longitudinal Vehicle Model Derivation

The core goal of this thesis is to develop an optimal method of being able to follow another tractor-trailer in a fuel efficient method. It is therefore important to have an accurate equation that can describe the driving forces of a class-8 vehicle. Figure 2.2 shows the basic driveline model relating engine speed to wheel speed. This version of the model has a couple of implicit assumptions:

- no gear slip
- no shaft compliance

These assumptions greatly simplify the driveline model without a substantive sacrifice in model fidelity.

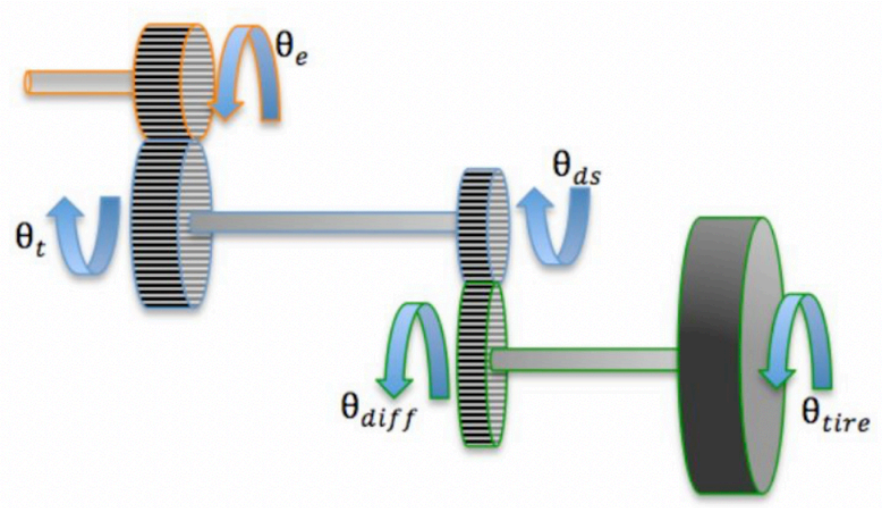

Figure 2.2: Class-8 Vehicle Powertrain Model [9]

By applying newton's second law to the entire powertrain, and applying the resulting force to the vehicle FBD shown in Figure 2.3, the resultant equation is Equation (2.1)

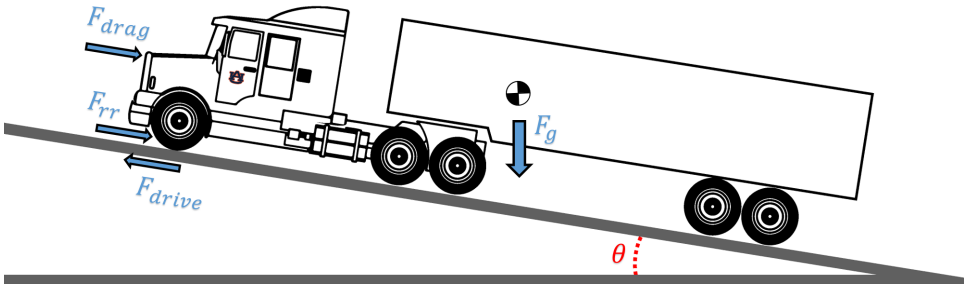

Figure 2.3: Class-8 Vehicle FBD [17]

$$M_{eff}\ddot{X} + B_{eff}\dot{X} + D\dot{X}^2 = \frac{\tau_{eng} * \eta_{diff} * \eta_{trans}}{r_{eff}} - F_{rr} - F_{grade} \tag{2.1}$$

In the above equation, F_{rr} is the force due to rolling resistance and F_{grade} is the force due to grade and can be written as Equation (2.2)

$$F_{grade} = (M_{tractor} + M_{trailer}) * g * \sin(grade) \tag{2.2}$$

While methods of reducing rolling resistance are not investigated in this work, it is worth noting that approximately 15-30% of a class-8 vehicles energy goes into overcoming rolling resistance [18].

In Equation (2.1) the effective mass and effective damping, M_{eff} and B_{eff} respectively, are both functions of the current vehicle gear and can be written as

$$M_{eff} = (M_{tractor} + M_{trailer}) + \frac{J_{diff}}{R_w^2} + \frac{J_{eng}\eta_{diff}^2\eta_{trans}^2}{R_w^2} \tag{2.3}$$

$$B_{eff} = \frac{B_{diff} + B_{trans} * \eta_{diff}^2 + B_{eng} * \eta_{diff}^2 * \eta_{trans}^2}{R_w^2} \tag{2.4}$$

It is important to make a brief note on Equation (2.1).The terms M_{eff} and B_{eff} vary with the selected gear which requires one of two things to occur. In the optimization horizon, it must be assumed that the gear is constant over the entire horizon, or the current gear must

be made a controllable parameter. Because the Auburn platooning system does not have control over the current gear selection, this thesis assumes that the gear will stay constant over any forward prediction utilizing Equation (2.1). Since the longitudinal dynamics of the vehicle have been derived, the following sections will now cover specific relationships within the vehicle powertrain that provide the relationship between wheel speed and fuel-consumption.

2.1.1 Engine Map

Traditionally, platooning applications are focused on maintaining a rigid inter-vehicle distance, commonly called headway, between two vehicles. In order to accomplish this, all a controls engineer would need is a longitudinal model of the vehicle like the one derived in the previous section. This thesis however is not singularly focused on maintaining a rigid headway between vehicles, but rather maintaining a nominal headway gap in a fuel-efficient manner. Since a key part of the optimization is generating an optimal velocity profile over uneven terrain, it is necessary to develop a relationship between a vehicle's velocity and fuel consumption. This section outlines the model derivation and validation for a velocity to fuel-rate model.

The first step in establishing the speed to fuel-rate relationship is validating the relationship between wheel speed and engine speed. This is an important relationship to validate because the engine speed is directly related to peak engine torque and fuel consumption. Using a very basic driveline model in which it is assumed there is no gear slip or wheel slip, engine speed can be calculated from wheel based speed using Equation (2.5)

$$\omega_{engine} = (\pi/30) * \frac{(\eta_{trans}\eta_{diff})}{r_{eff}} * \omega_{wheel} \tag{2.5}$$

where η_{diff}, η_{trans} and ω_{wheel} are the differential gear ratio, transmission gear ratios and wheel speed respectively. Figure 2.4 shows that Equation (2.5) actually yields a smoother estimate of the engine speed than the CAN bus. This data comes from a 7Km long run

where the unarmored M915 was tasked with maintaining 55MPH (24.58 m/s). The terrain for this test was rolling hills and is further outlined in section 5.2.2.

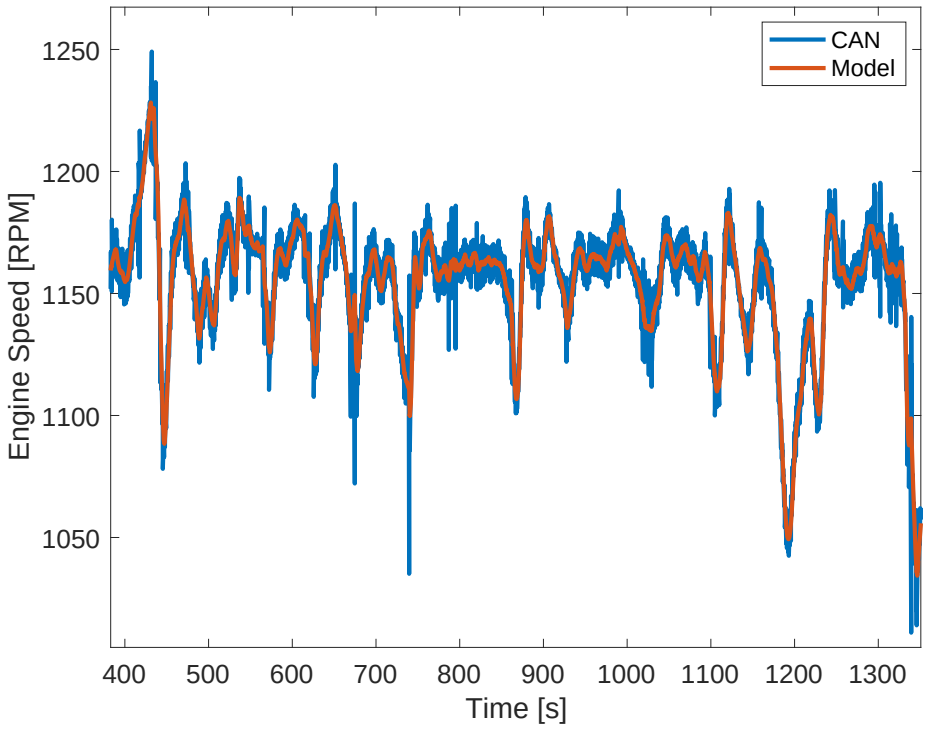

Figure 2.4: Modeled Engine Speed vs CAN Engine speed

The next step is creating a relationship between engine speed and peak engine torque. Through empirical analysis of previous platooning data, the operating range for the engine has been observed to be between 1000 and 1800 RPM. The maximum possible engine torque can be calculated as a function of engine speed. A least squares fit was used to determine the coefficients of a third order polynomial the fits engine speed to peak engine torque. Figure 2.5 shows the final results of the least squares fit. The least squares fit has a peak error of 1.609% which is acceptable for this application.

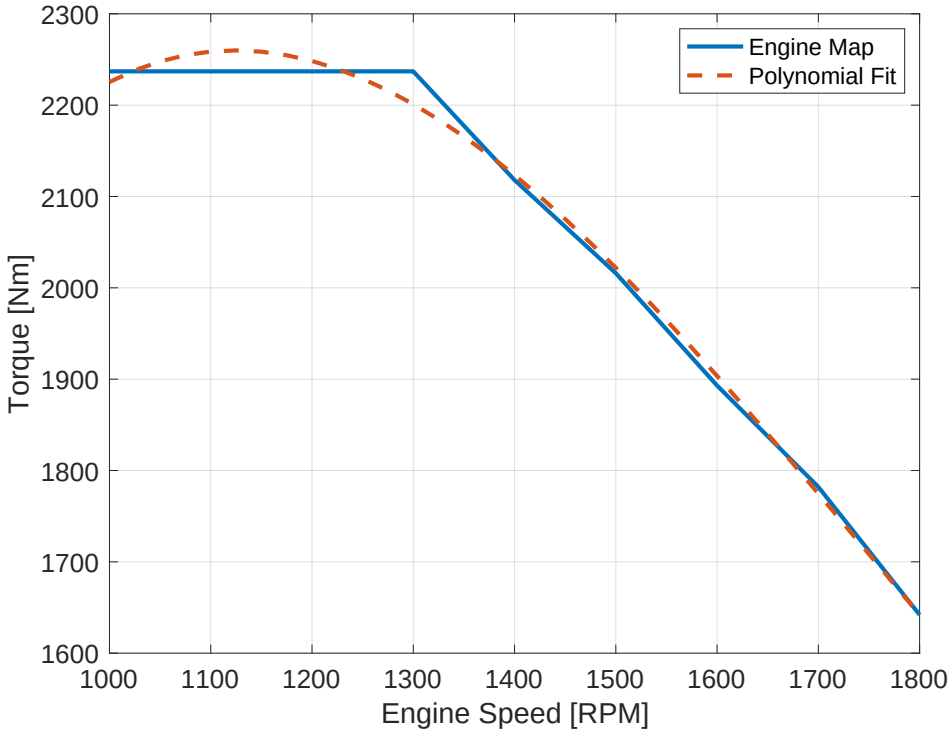

Figure 2.5: Polynomial Fit to Peak Torque

The engine polynomial displayed in Figure 2.5 is defined by Equation (2.6).

$$T_{max} = c_1\omega_e^3 + c_2\omega_e^2 + c_3\omega_e + c_4 \tag{2.6}$$

Equation (2.6) alone is only moderately useful however since it only provides the peak engine torque at a specific engine speed. Equation (2.7) then provides the relationship from peak torque to engine torque, where $u_{throttle}$ is the normalized throttle position as reported by the CAN bus.

$$T_{engine} = T_{max} * u_{throttle} \tag{2.7}$$

Figure 2.6 presents the calculated engine torque from Equation (2.7). Over the course of a 75 mile run, the maximum error between the calculated torque and measured torque was 7%. This peak error occurred during a gear shift which is important to note, because

Equation ((2.5)) breaks down while the clutch is disengaged. Besides scenarios such as gear shifting, the mean torque error over the evaluated dataset was 12.53 N-M or 1.21%.

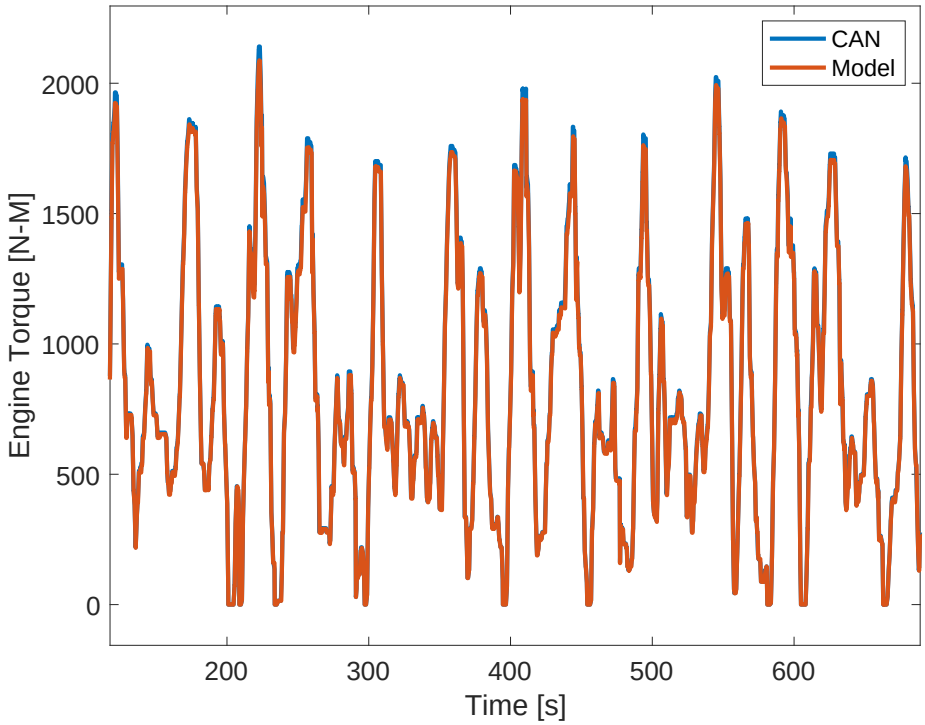

Figure 2.6: Estimated Engine Torque Evaluation

The final link from wheel-speed to fuel-rate is from engine torque to fuel-rate. To make this link the Brake Specific Fuel Consumption (BSFC) map must be determined. The BSFC number provides the ratio of fuel-rate to power. It is not sufficient however to say that the BSFC is a single number, but rather a 3-dimensional map that that changes as a function of engine speed and engine power. These 3-dimensional maps are usually well known by OEM's but are not easily accessible to 3rd party researchers that are not working in concert with the OEM. Since Auburn does not have access to the BSFC map, a process to approximate the BSFC must be used.

To begin building a BSFC map, one of the M915's used for testing was run along a stretch of hilly terrain 5 times. During these runs all J1939 CAN data were logged. Since BSFC is a relationship between engine speed, engine power and fuel-rate, two preliminary plots are generated. The first plot is Figure 2.7 which displays the relationship between engine

speed and engine power. The second plot, Figure 2.8 displays the relationship between the engine's fuel-rate versus engine speed. The key benefit of viewing these plots individually versus engine speed is to recognize that both engine power and fuel-rates increase near the top of their respective Y-axes. This is a trend that is harder to visualize on the 3-dimensional plot where one could easily mistake the 3-dimensional plot as yielding a perfectly linear relationship rather than a non-linear relationship.

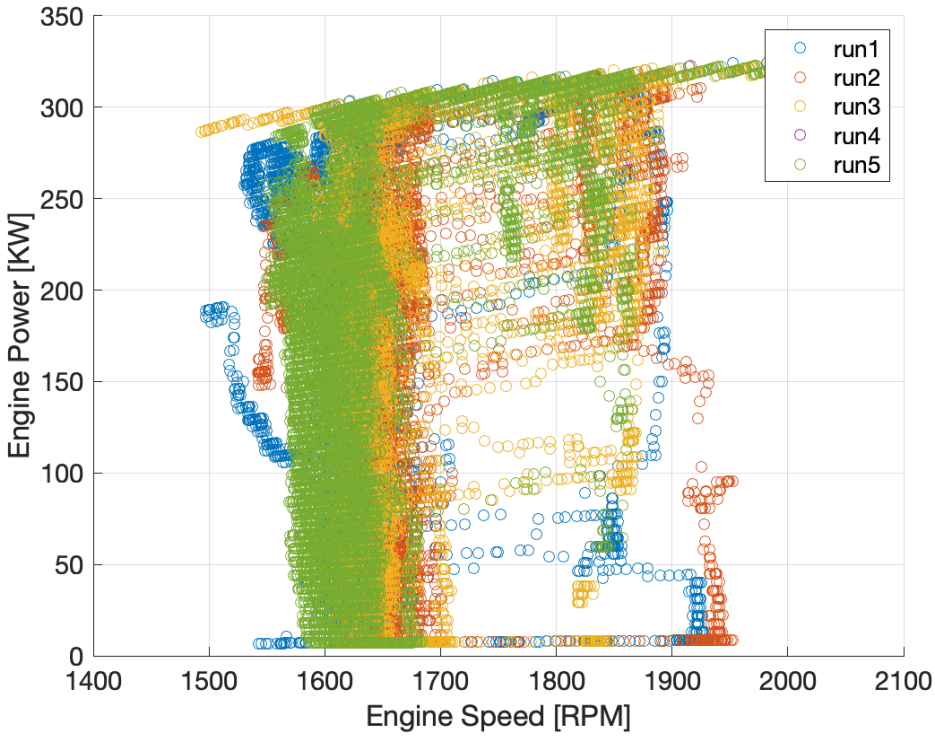

Figure 2.7: Engine Power vs Engine Speed

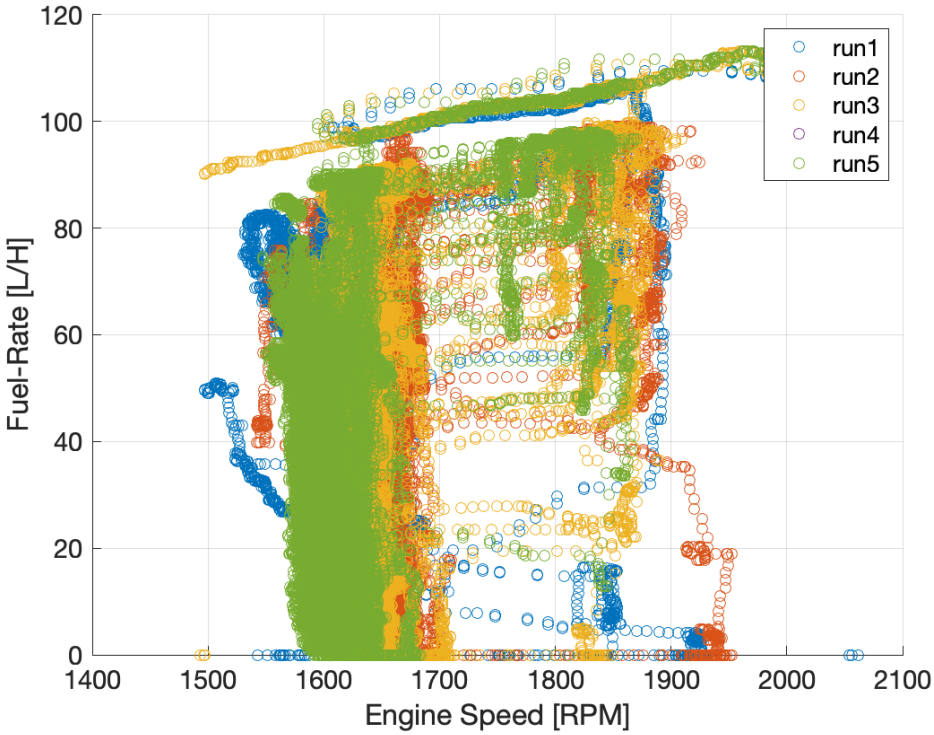

Figure 2.8: Fuel-Rate vs Engine Speed

In order to process the data to generate a BSFC map, Figures 2.7 and 2.8 are combined into one 3-dimensional plot presented as Figure 2.9. It is from this data that the relationship between engine power, engine speed and fuel-rate will be derived. Because the relationship between between fuel-rate and engine-power isn't highly non-linear, both a linear and non-linear polynomial will be evaluated for their ability to predict fuel-rate given the current engine power demand and engine speed. The linear and non-linear polynomials are described in Equations (2.8 - 2.9) respectively, where the coefficients b_i are to be determined through a least-squares approach.

$$\dot{V}_{fuel} = P_{eng} * b_0 \tag{2.8}$$

$$\dot{V}_{fuel} = P_{eng}^2 * \omega_{eng} * b_0 + P_{eng} * \omega_{eng} * b_1 + P_{eng} * b_2 \tag{2.9}$$

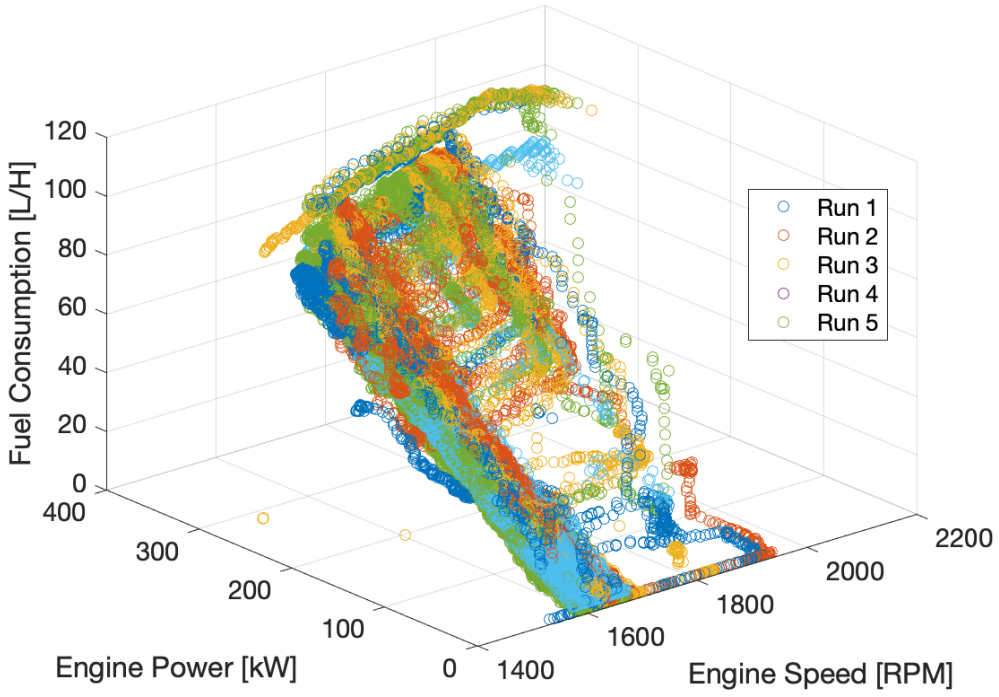

Figure 2.9: Fuel-Rate vs Engine Speed

The least squares process resulted in the coefficients listed in table 2.2

Table 2.2: Least-Squares BSFC Coefficients

Coefficients	Coefficients Value
Linear: b0	.2819
Non-linear: b0	-7.699e-06
Non-linear: b1	2.1131e-07
Non-linear: b2	0.2101

These two fuel rate models were then validated against a different dataset driven by the same vehicle to ensure that the fuel-rate model was not over-fitting the data used in the least-squares analysis. Figure 2.10 presents a comparison between the linear, non-linear and measured fuel rate. It becomes obvious via visual observation that the non-linear model

tracks the fuel-rate much better at the higher and lower ends of the fuel consumption spectrum. Figure 2.11 shows the fuel-consumption error from both the linear and non-linear model over the same dataset analyzed in figure 2.10.

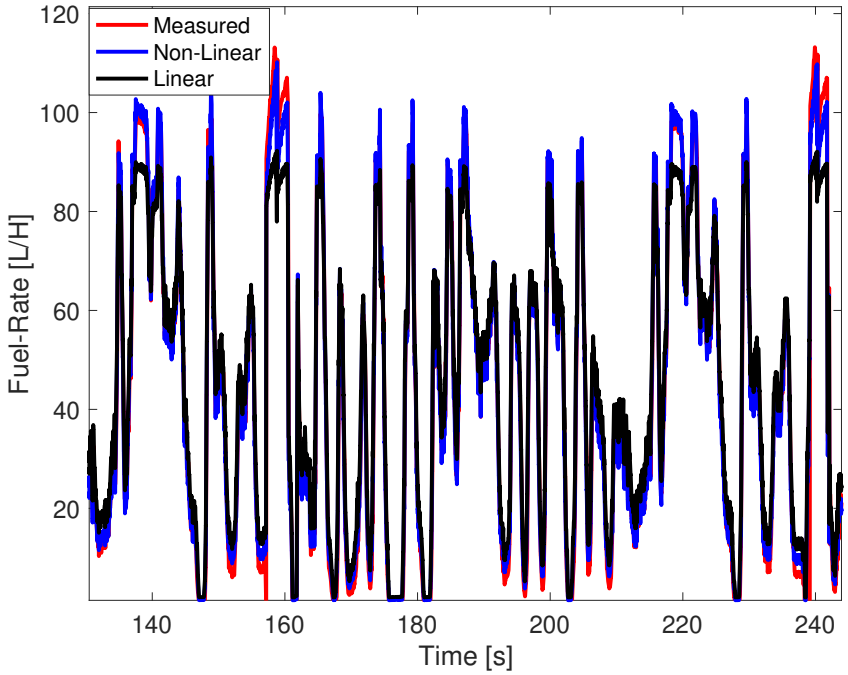

Figure 2.10: Comparison of Fuel-Rate Models

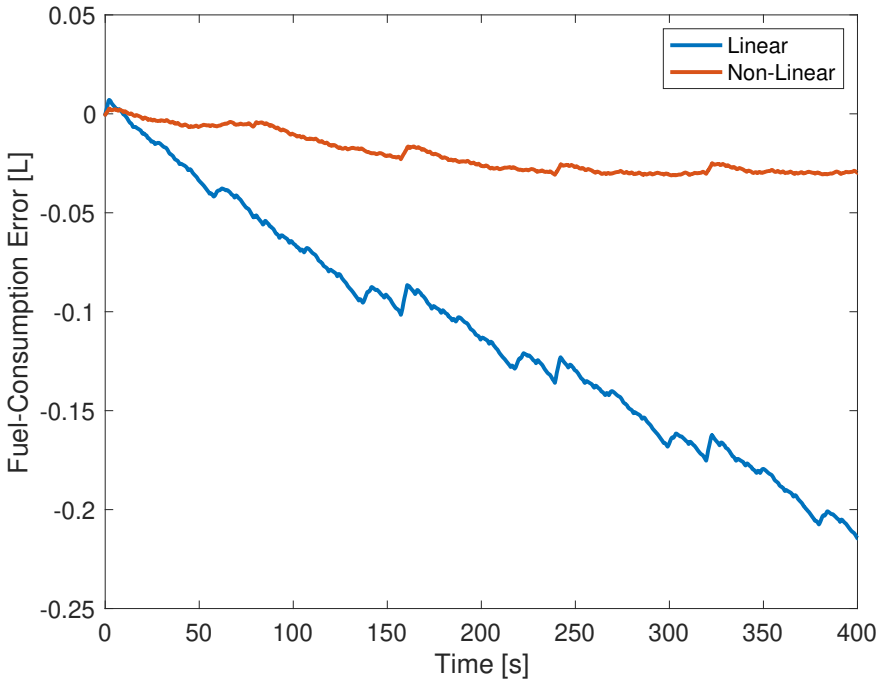

Figure 2.11: Comparison of Fuel Model Residuals

Figure 2.11 clearly demonstrates that the non-linear fuel model outperforms the linear fuel model. The non-linear model was therefore desired as the preferred model. However, during the development of the real-time application, there were challenges with software crashes when using the non-linear model. Therefore, due to time constraints on vehicle and personnel time constraints the linear model was then used for the remainder of the work presented.

To evaluate the efficacy of using the linear model instead of the non-linear model, extensive analysis was done in reference to previous fuel-campaigns performed by the Auburn team. The linear fuel model was applied to 10 test runs conducted with the research presented in [19]. Each test run was approximately 48 miles long and took place on I-85 between Opelika and Tuskegee, Alabama. Table 2.3 demonstrates that there is still sufficient accuracy with the linear fuel model to have confidence in the NMPC algorithm that relies on this relationship.

Table 2.3: Estimated Fuel Results Using Linear Fuel Model

Run #	Truck #	Estimated Fuel Consumption	CAN Fuel Consumption	% Error
1	A2	17.234	17.2929	0.34
2	A2	13.7535	13.8775	0.893
3	A2	15.9683	16.0382	0.436
4	A2	15.6977	15.7722	0.472
5	A2	16.1575	16.2885	0.804
6	A2	15.0996	15.2406	0.925
7	A2	16.009	16.2387	1.414
8	A2	16.3426	16.3566	0.085
9	A2	16.352	16.4775	0.762
10	A2	17.1104	17.108	0.104

2.2 Hardware Overview

The hardware in the platooning vehicles are the physical devices that provide external measurements, perform communication functions or process incoming/outgoing information. The platooning system developed by the Auburn team was designed to be minimally invasive and easy to integrate into existing vehicles without high cost. An overview of the hardware setup is shown in Figure 2.12. While the Auburn vehicles are capable of occasional SAE level-2 performance, the primary function of platooning is in the SAE level-1 autonomy domain [20]

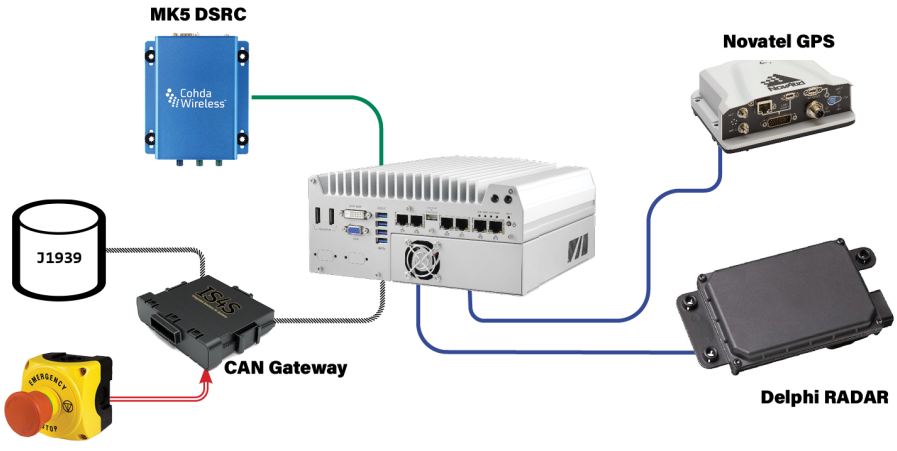

Figure 2.12: Class-8 Vehicle Powertrain Model [17]

The key pieces of hardware used in this thesis are

- A Nuvo-5095GC ruggedized computer. This computer runs a Linux OS: Ubuntu 16.04. The computer also comes equipped with two PCAN-miniPCIe chips that allow for the reading/writing of CAN messages in real time. The computer handles all data processing and control generation and is responsible for running the NMPC algorithm.

- Cohda Wireless MK5 OBU. This radio is responsible for transmitting relevant vehicle states and raw GPS observables from the lead vehicle to all other vehicles. This radio link establishes the V2V capabilities of the Auburn platooning system and serves as a method of calculating the position of a vehicle within the platoon.

- Delphi ESR RADAR. The Radar is responsible for scanning and returning high frequency range, range-rate, and bearing measurements from objects located in the platooning trucks direction of travel.

- Novatel FlexPak. The Novatel GPS receiver receives raw L1/L2 GPS signals from a Novatel Pinwheel and provides GPS position and velocity measurements. These measurements are also used to provide an accurate Relative Position Vector (RPV) to the lead truck.

- CAN gateway. The CAN gateway is a custom device built by Integrated Solutions for Systems (IS4S). This device physically separates the Auburn platooning system from the vehicle CAN bus. An emergency stop button can be pressed to kill any communication to/from the vehicle in the case of an emergency.

2.3 Software Architecture

The bulk of the CACC algorithms implemented on the Auburn platforms are written in C++/Python. Because interfacing software processes directly can be difficult, a middle-ware

was selected that allows for a standard interface between one software process to another. The middle-ware used in this thesis is called the Robotic Operating System (ROS) [21].

With ROS, several different software processes can easily be written to handle a specific task. Every task is known as a node and is represented by a gray oval in Figure 2.13. Each software process will publish a standard ROS message which is accessible to any other software using ROS to send and receive data. This publishing process is represented by the black arrow between ovals and is called a ROS topic.

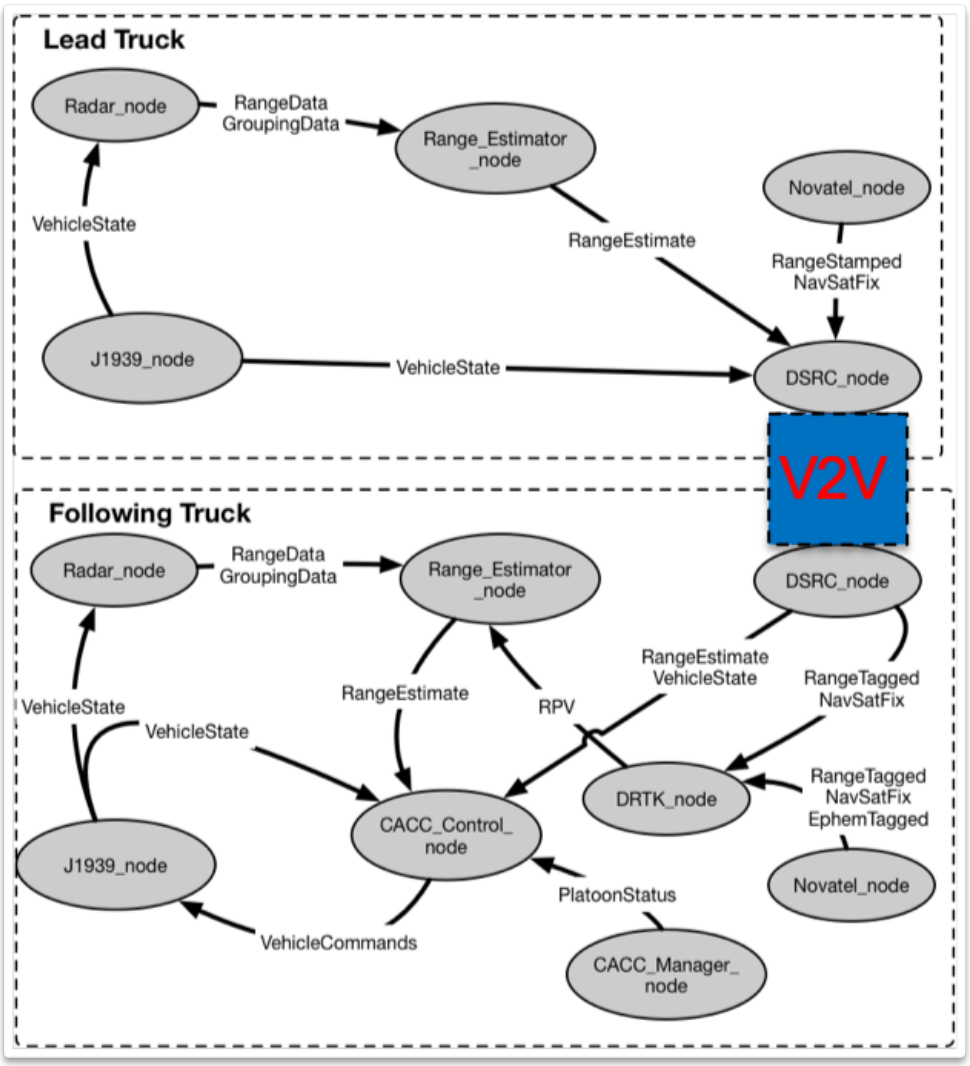

Figure 2.13: Auburn CACC Software Overview

The software processes shown in Figure 2.13 can be put into 4 different categories: estimation, control, safety and communication.

Estimation:

- DRTK node: The DRTK node uses raw GPS observables from both the lead vehicle and following vehicle to generate a relative position vector (RPV). This RPV cancels out atmospheric error and generates a centimeter level accurate relative position measurement. This measurement is only updated at 2Hz within the system architecture.
- RADAR node: The RADAR node receives signals such as steer angle and velocity from the truck computer. The Delphi RADAR uses the steer angle and velocity signals to pre-filter the RADAR data and return only the range, range-rate, and bearing of object in the path of the platooning vehicle.
- Range Estimation node: the range estimation node is a Kalman filter (KF) that combines the provided sensor measurements including DRTK, RADAR and relative wheel speeds into an optimal estimate of the true vehicle headway.

Control:

- CACC Control node: The CACC control node takes in relevant signals from various nodes such as headway information, current vehicle states and current platoon status. The control architecture running at the time (H_∞, PID , MPC etc.) will then generate the longitudinal torque or steer angle command.

Communication:

- J1939 CAN node: The J1939 CAN node reads in all of the CAN communication data being passed through the vehicle. The J1939 CAN node also writes all the vehicle commands generated in the Control node to the vehicle CAN bus.
- DSRC node: The DSRC node is responsible for passing relevant information such as current vehicle states and raw GPS observable from one vehicle to another. Every

message sent through the DSRC node is stamped with the vehicles platform ID which corresponds to its position within the platoon.

Safety:

- Convoy Manager: The convoy manager node recieves messages from almost every software process. The main responsibility of this node is to perform "health checks" to make sure all processes are publishing at the correct frequency. If the convoy manager detects any anomalies, the system will automatically disable and require the driver to take over control.

Chapter 3

Methods of Generating Terrain Profiles

One of the critical aspects of being able to perform NMPC over rolling terrain is to have a map with sufficient resolution to effectively optimize the velocity of the vehicle. This thesis will investigate two ways to produce a terrain profile. The first method is using GPS velocity measurements in a local coordinate frame to estimate the road grade. The second method is to difference consecutive GPS odometry measurements to estimate road grade. Since it is important that obtaining terrain profiles does not create any extra cost or technical burden for professional trucking fleets, it was decided to use only measurements already captured on most commercial vehicles. In this thesis, GPS measurements were generated by a Novatel PwrPak 6 with an L1/L2 Novatel Pinwheel receiver. The accuracy of these methods of map generation will be evaluated and the final terrain map used is presented.

3.1 Map From Novatel GPS Velocity

One of the easiest and computationally efficient methods for determining the grade of a road is to use the GPS velocity output of the GPS receiver. The Novatel receiver used in this thesis outputs a GPS velocity in the ECEF coordinate frame. The GPS velocity is then rotated into a ENU coordinate frame. The ENU coordinate frame is a flat coordinate frame centered about a local coordinate, in this case the center of the NCAT skidpad, located at (32.595534,-85.295259). ENU coordinate frames are commonly used in navigation applications because it allows easy interpretation of position and velocity data in units such as meters and feet. Equation (3.1) describes the relationship between the ECEF coordinate frame and the ENU coordinate frame.

$$\begin{bmatrix} eastVel \\ northVel \\ upVel \end{bmatrix} = \begin{bmatrix} 1 & 0 & 0 \\ 0 & cosd(90+refLong) & sind(90+refLong) \\ 0 & -sind(90+refLong) & cosd(90+refLong) \end{bmatrix} * \begin{bmatrix} cosd(90-refLat) & sind(90-refLat) & 0 \\ -sind(90-refLat) & cosd(90-refLat) & 0 \\ 0 & 0 & 1 \end{bmatrix} * \begin{bmatrix} xVel \\ yVel \\ zVel \end{bmatrix} \quad (3.1)$$

Once the velocity has been transformed into the ENU coordinate frame, the grade can be calculated using Equation (3.2).

$$grade = \arctan\left(\frac{upVel}{\sqrt{eastVel^2 + northVel^2}}\right) \quad (3.2)$$

Figure 3.1 shows the estimated grade using Equation (3.2) during a drive of highway-280 in Alabama. While the measurement seems noisy, the SNR for the shown data is 59.4362. Typically a SNR greater than 45 db-Hz is considered good [22]. Figure 3.2 is the same plot as Figure 3.1 however it is on a smaller timescale. This provides an easier view of the actual grade estimate from the GPS velocity measurement.

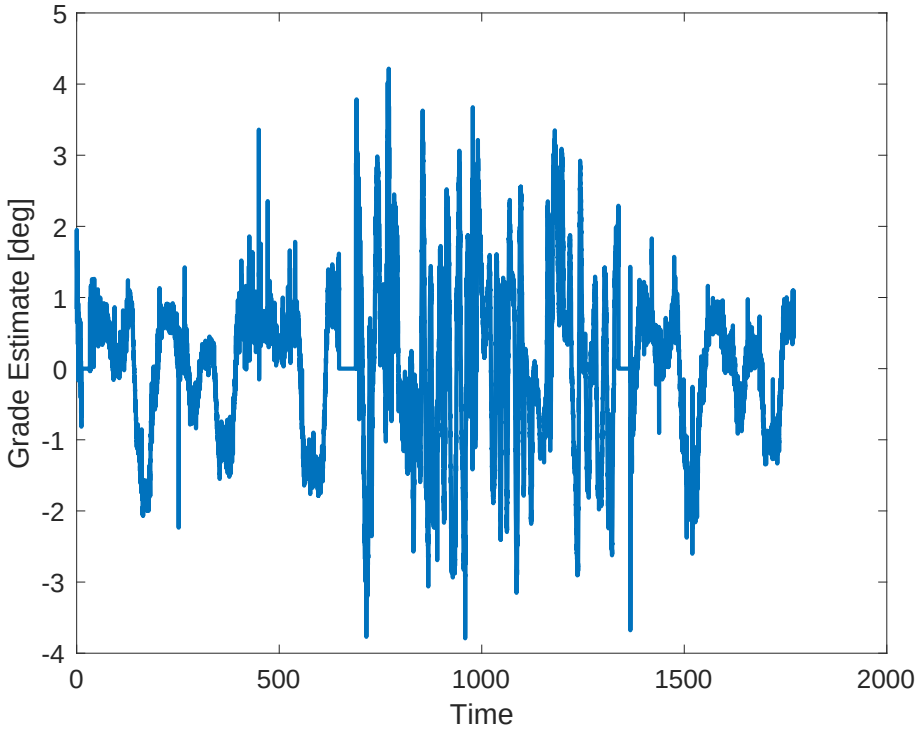

Figure 3.1: Grade Estimate of Terrain Using GPS Velocity

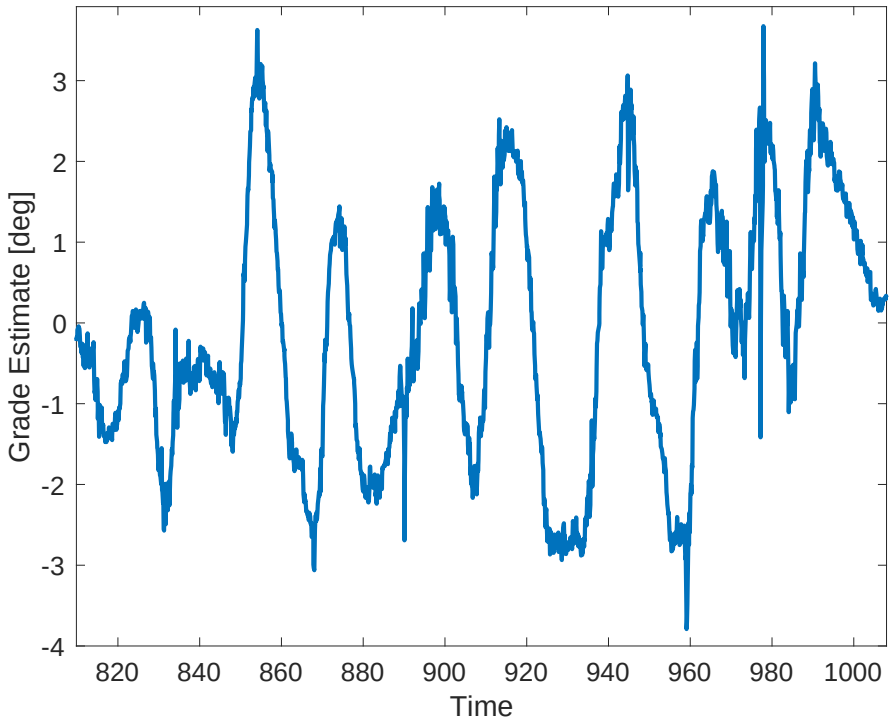

Figure 3.2: Zoomed Grade Estimate from GPS Velocity

Using GPS to generate a grade map is the most tractable for real world use. GPS receivers are becoming a common sensor on modern class-8 vehicles, especially with the introduction of Electronic Logging Devices which enforce Hours of Service laws and more advanced ADAS systems. Using this method to generate the final reference map seen in Figure 3.3 would not require the addition or expense of outfitting a truck fleet with any new sensors. A caveat with this method is that GPS velocity based grade estimate is not accurate at low speeds, however this issue is not likely to be of great concern since the target operational domain is highway driving.

The GPS velocity based grade estimate was previously evaluated against a profilometer and was seen to be comparable in signal quality. While there is no specific threshold criteria to define "accuracy", it is strongly desired that the relative error in slope values be minimal [14] which Figure 3.4 shows is achieved. If one wishes to smooth the GPS estimate, a low pass filter or signal smoother can be used.

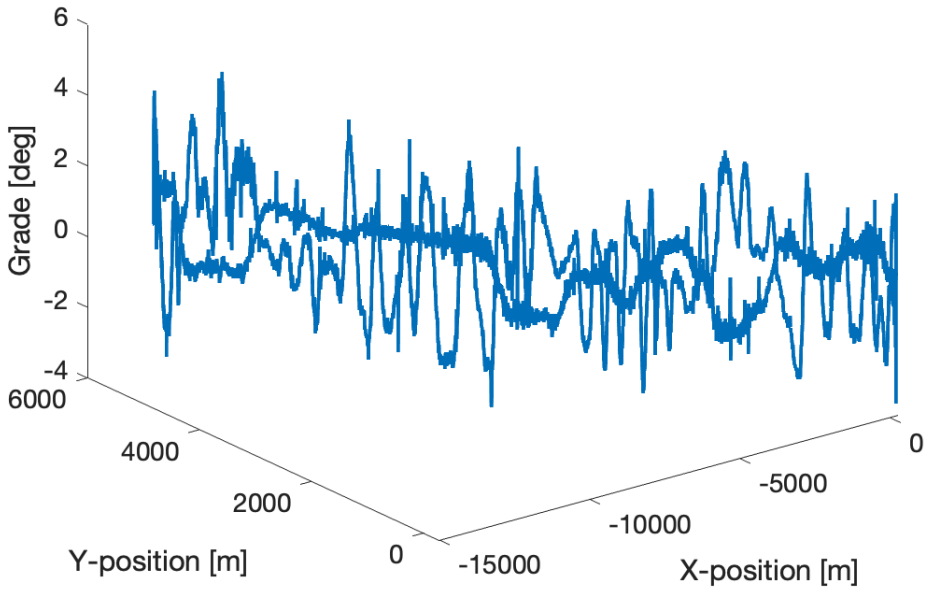

Figure 3.3: Final Terrain Map Using GPS Velocity

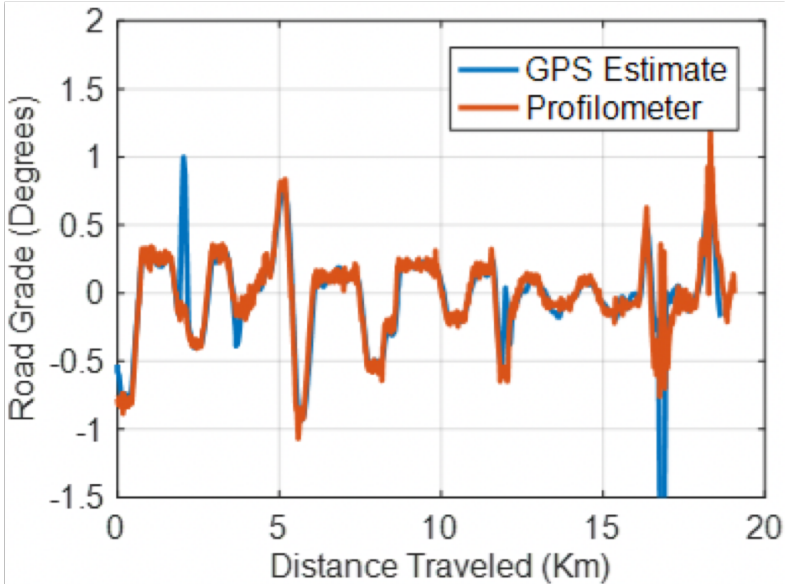

Figure 3.4: Comparison of GPS Velocity Grade vs Profilometer [23]

3.2 Map From Novatel Odometry

Odometry is a measure of a vehicle's position and velocity. In Section 3.1, GPS velocity was used to estimate the grade of the terrain it was driving on. This section aims to use the position data from the Novatel receiver to generate a grade map.

Figure 3.5 shows the output of the GPS receiver plotted in the ENU frame. In order to back out grade information, the position data between consecutive time epochs can be differenced. Equation ((3.3)) describes the processing of differencing measurement positions to try and get a grade estimate.

$$grade = \arctan \frac{\Delta z}{\sqrt{\Delta x^2 + \Delta y^2}} \tag{3.3}$$

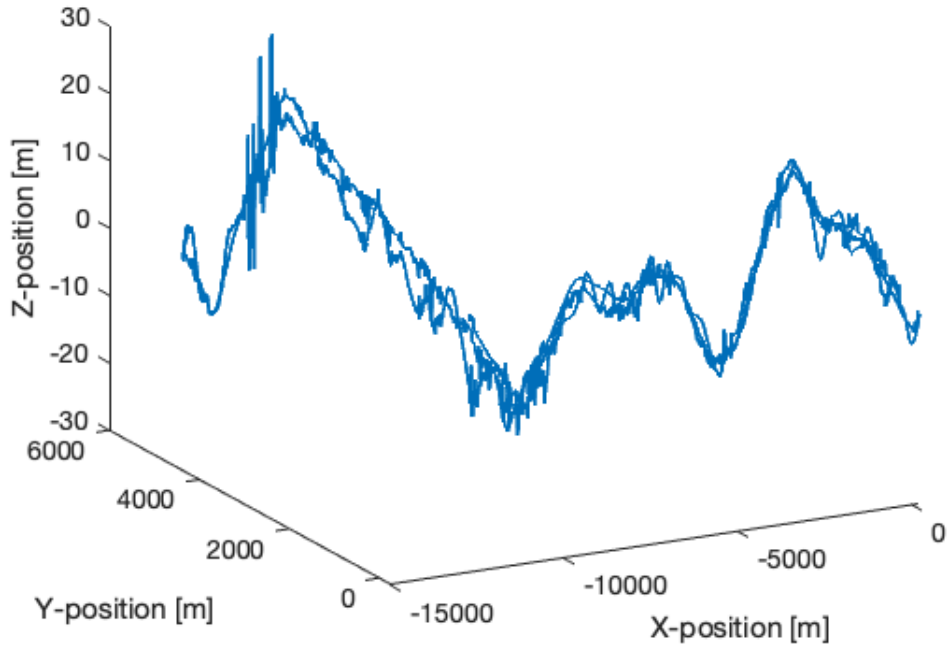

Figure 3.5: 3-D Map of a Section of Highway-280 in Alabama using Raw Novatel Odometry

Figure 3.6 shows the output of the odometry differenced grade. Its obvious that this map is not as accurate. The problem with this methodology is that any noise in a signal that is numerically differentiated will be amplified. In this case the noise was high enough to ruin the grade estimate.

In this chapter two methods of obtaining grade over any terrain were described. While these two methods were treated as distinct, the methodology of differencing vehicle odometry is essentially the same as using GPS velocity to calculate grade. The core distinction between the two methodologies is that there is no differentiation performed with the GPS velocity

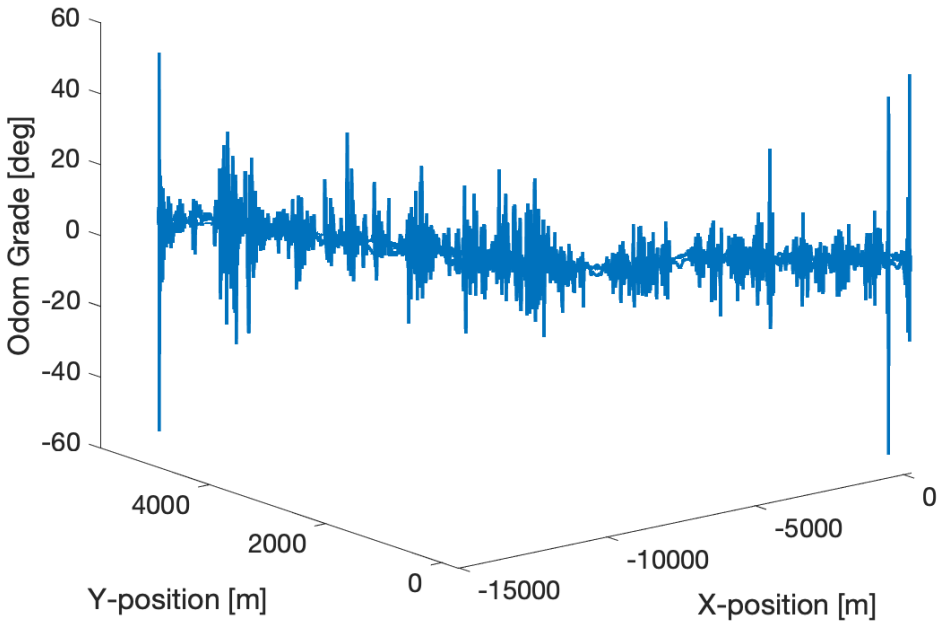

Figure 3.6: 3-D Map of Odom Differenced Grade

method. As a result, the method of calculating grade using GPS velocity was selected as the method of generating terrain profiles, and Figure 3.3 represents the terrain map used for the remainder of this thesis.

Chapter 4

Classical Platooning Controller Design

This chapter aims to outline the design methodology used to design the original Auburn PID control system. The original control law will be derived and shortcomings in the design process will be analyzed. Next, a more robust PID control methodology will be explored that uses the H_∞ to provide a form of structured optimal control.

4.1 PID Control Design

The goal of the longitudinal control system is strictly to maintain a desired headway. For ease of implementation with the original system, a PID controller was designed and implemented. Figure 5.2 remains a good description of the leader-follower problem to be solved in this section.

The control architecture can be best represented by Figure 4.1. In figure 4.1 h is the estimated headway, h_{ref} is the desired headway and T_{FF} is a feed-forward torque.

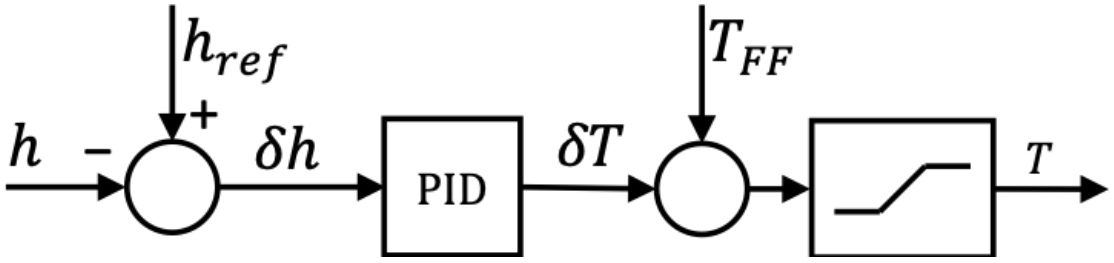

Figure 4.1: Classical PID Control Architecture [23]

The feed-forward torque is important in classical control methods as it can account for both non-linearities in the system and known disturbances to the system. In this case the T_{FF} term accounts for the air-drag term as well as the grade disturbance found in Equation (2.1) and is defined by Equation (4.1)

$$T_{FF} = (Dv_i^2 + (M_{tractor} + M_{trailer})g * \sin(grade)) * \frac{R_{eff}}{\eta_{diff}\eta_{trans}} \tag{4.1}$$

The PID block in Figure 4.1 calculates the commanded torque via the control law defined in Equation (4.2)

$$T_{pid} = K_P(h_{ref} - h) + K_I \int (h_{ref} - h)dt + K_D * (V_{i-1} - v_i) \tag{4.2}$$

By plugging Equation (4.2) into Equation (2.1) the Characteristic Equation (C.E.) of the system can be identified. By choosing three desired time constants one can derive the desired C.E. that follows the form of Equation (4.3)

$$s^3 + (\frac{1}{\tau_1} + \frac{1}{\tau_2})s^2 + (\frac{1}{\tau_1\tau_2} + \frac{1}{\tau_2\tau_3} + \frac{1}{\tau_1\tau_3})s + \frac{1}{\tau_1\tau_2\tau_3} = 0 \tag{4.3}$$

with the time constants used in this work listed in Table 4.1

Table 4.1: Desired Time Constants for PID Pole Matching

τ_1	12.5s
τ_2	6.25s
τ_3	2.5s

It is then a simple process to derive the control law for this system with the final control gains taking the form of Equations (4.4 - 4.6)

$$K_P = -\frac{M_{eff}R_{eff}}{\eta_{diff}\eta_{trans}}(\frac{1}{\tau_1\tau_2} + \frac{1}{\tau_2\tau_3} + \frac{1}{\tau_1\tau_3}) \tag{4.4}$$

$$K_I = -\frac{M_{eff}R_{eff}}{\eta_{diff}\eta_{trans}}(\frac{1}{\tau_1\tau_2\tau_3}) \tag{4.5}$$

$$K_D = -\frac{M_{eff}R_{eff}}{\eta_{diff}\eta_{trans}}(\frac{1}{\tau_1} + \frac{1}{\tau_2}) \tag{4.6}$$

While this control strategy is easy to implement and requires no knowledge about the lead vehicle in the platoon, it does not guarantee string stability for the platoon. While string stability can be defined in several ways, this work uses the mathematical definition of Equation (4.7) to define string stability.

$$\left\| \frac{u(i)}{u(i+1)} \right\|_{\infty} < 1 \; \forall \; \omega > 0 \tag{4.7}$$

This mathematical description of string stability states that the output acceleration of the following vehicle must be smaller in magnitude than the commanded acceleration of the preceding vehicle across all frequencies. Figure 4.2 displays the string instability of the system even while under gradual grade disturbances.

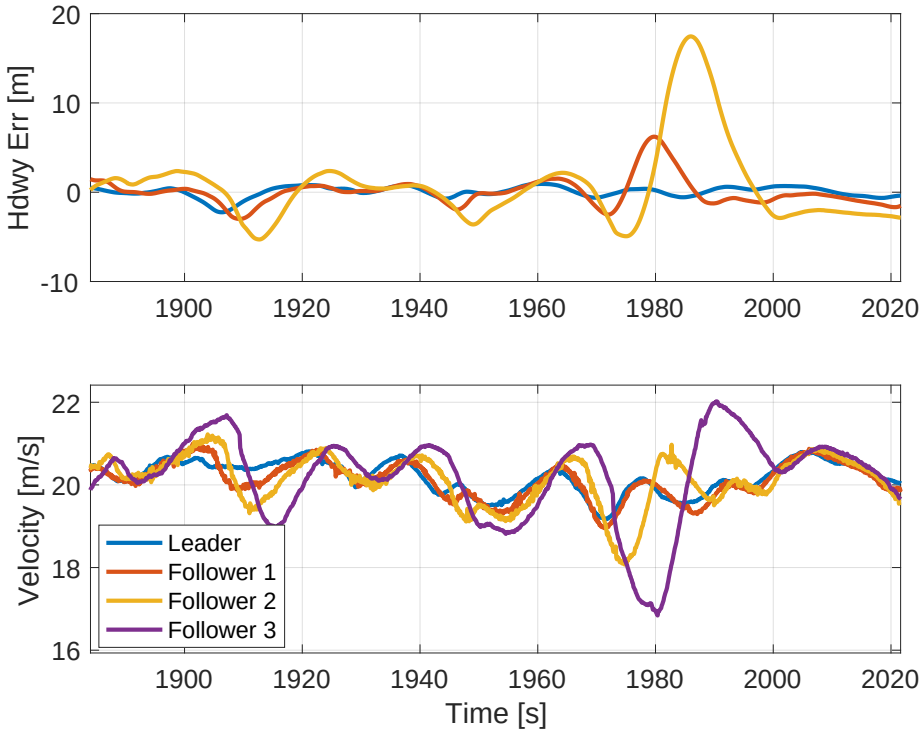

Figure 4.2: Classical PID String-Instability

4.2 H_∞ Control Design

The goal of the H_∞ design is to specifically account for the string stability requirement while designing the controller. While H_∞ design can be used on a fixed-structure control architecture such as a PID controller [24], the design process is quite different than that of a tradition pole matching technique. The rest of this section will provide an overview of the design process for the H_∞ platooning controller which takes heavy inspiration from [6, 7].

The first step in the H-infinity process is to generate an accurate model of the system. Figure 4.3 provides the system model for any vehicle in an $N - length$ platoon denoted as vehicle i.

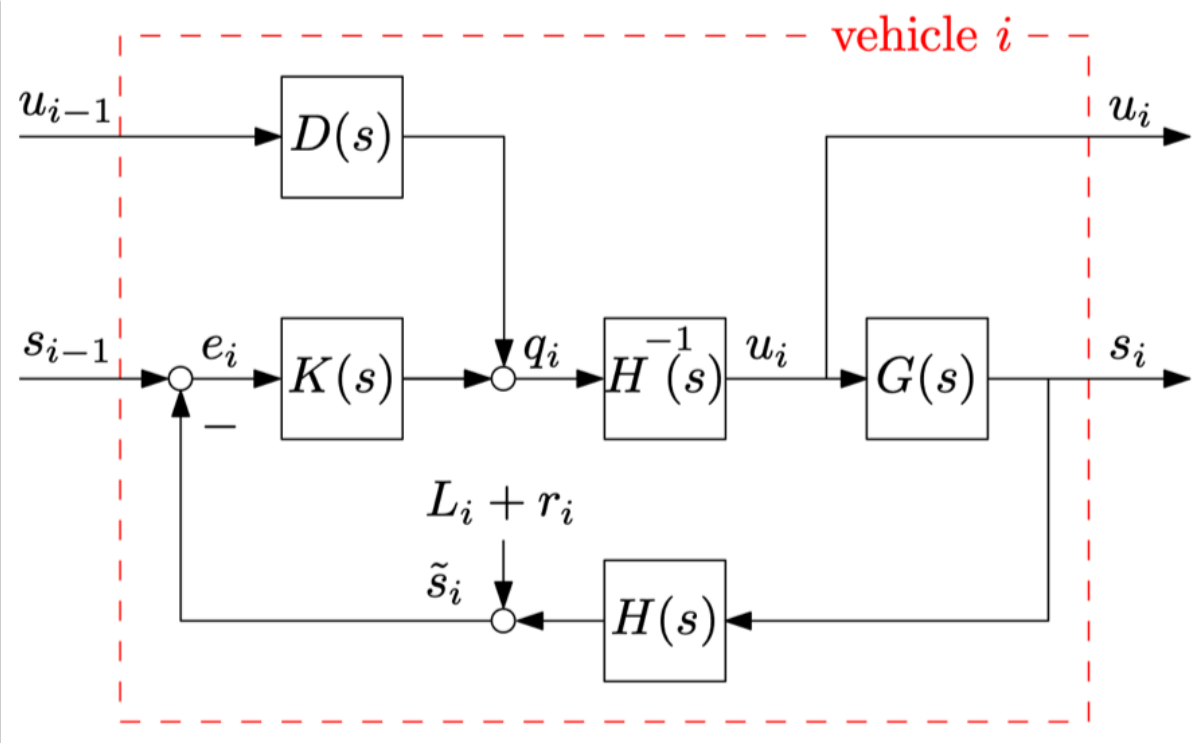

Figure 4.3: Platooning H-inf Block Diagram [7]

In this figure $D(s)$ is the communications delay between the preceding vehicle $i-1$ and the following vehicle. This delay is approximated as a second order Pade delay [12]. $K(s)$ is the controller for the system we wish to design which takes the form of a PID controller in this scenario. $H(s)$ is the spacing policy between vehicles with a time based gap policy

rather than a distance based policy. Finally, $G(s)$ is the system dynamic model. In this work the entire driveline model is considered a feed-forward term thus abstracting out mass and gear parameters to allow the controller to be used across a non-homogeneous platoon. $G(s)$ is therefore defined as Equation (4.8)

$$\frac{s_i}{u_{cmd}} = \frac{1}{s^2(\tau s + 1)} \tag{4.8}$$

where s_i is the position of vehicle i and u_{cmd} is the commanded acceleration of the platform.

Typically the H_∞ problem can be generalized into a structure defined by Figure 4.4 where w and z are exogeneous inputs and outputs respectively. Additionally, y and u are the system outputs and control input.

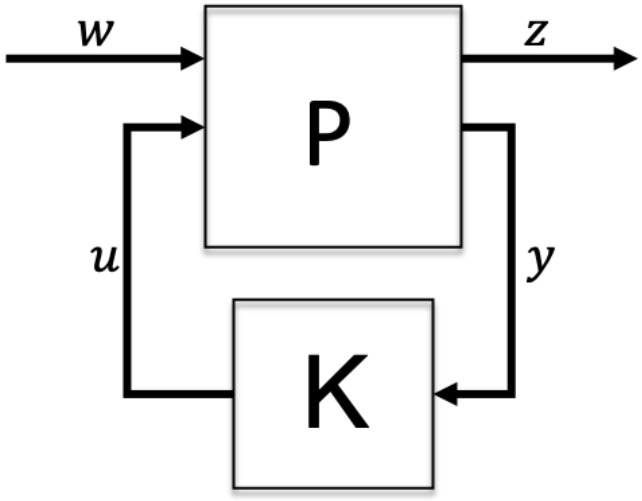

Figure 4.4: Generic H_∞ Structure

In this formulation the design objective is summarized using Equation (4.9) [25].

$$\|T_{w\to z}\|_\infty \tag{4.9}$$

s.t. K stabilizes P internally

This equation states that the objective of the H-infinity design process is to minimize the H_∞ norm of the $w \to z$ signal.

The H_∞ norm can be changed by adding frequency based weightings to the exogeneous outputs z of the system. In this thesis, the exogeneous outputs to be weighted were the system error and control actuation signals. The corresponding input signals were selected to be the preceding vehicle's acceleration and position. The corresponding block diagram with the weighted outputs is outlined in Figure 4.5.

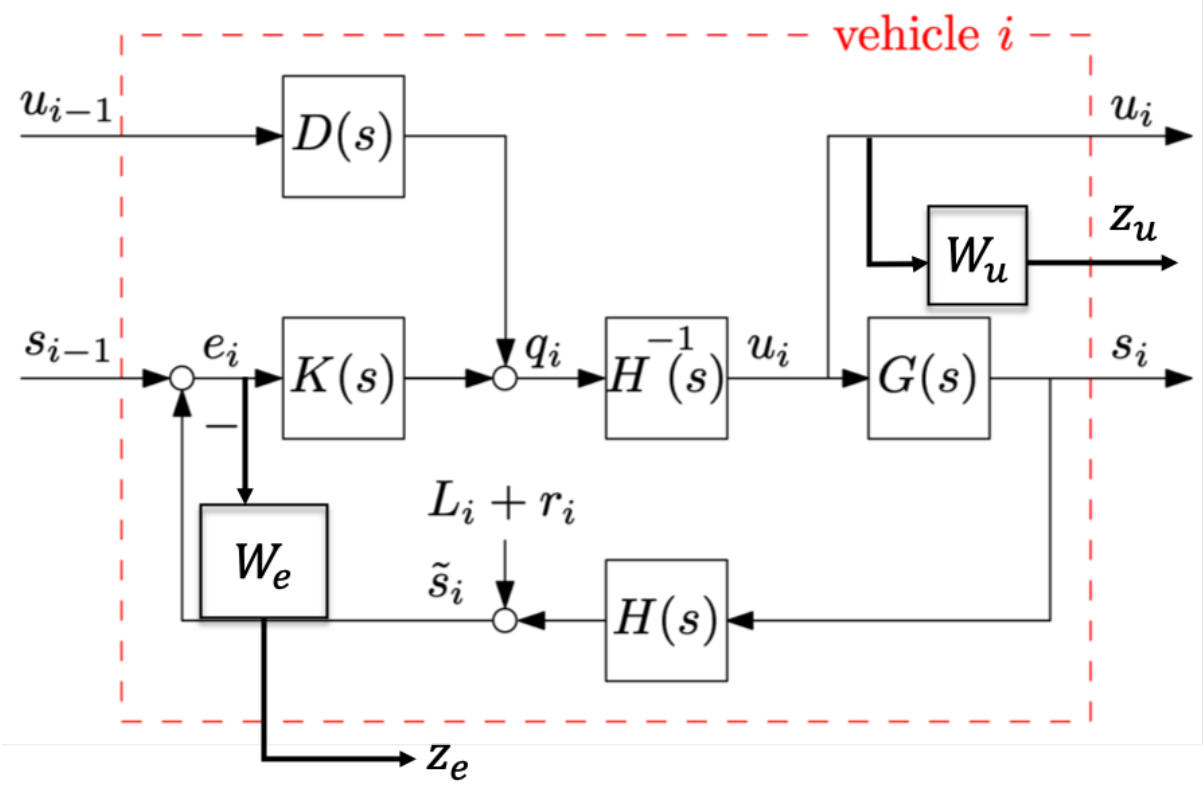

Figure 4.5: Weighted H-inf Block Diagram [7]

The frequency based weightings set the relative importance of every signal across all frequencies. For instance if one wishes to limit high-frequency control actuation, the gain w_u would be roughly equivalent to a high-pass filter where the system gain increases with frequency. The weight W_e is slightly easier to generate as it should take the shape of the desired open-loop bode plot. To generate this function define the desired C.E. and then follow the steps in Equation (4.10).

$$C.E. = s^2 + 2\zeta\omega_n s + \omega_n^2 \tag{4.10}$$
$$W_e = \frac{C.E.}{1 - C.E.}$$

Because the system dynamics outlined in Equation (2.1) are all encompassed as a feed-forward torque, the control gains do not need to be re-calculated for every gear. The only time the control gain would need to be recalculated is when the desired headway is changed because the spacing policy $H(s)$ is specifically accounted for within the design model. Using the MATLAB *hinfstruct* command in conjunction with the *icsys* function to build the model, a PID controller was successfully designed for the system. The resulting control gains are listed in table 4.2. These control gains closely align with those derived in other works such as [6, 7, 12].

Table 4.2: H_∞ Design Control Gains

Gain Type	Controller Gain
K_P	.224
K_I	.034
K_D	.784

Next it is important to make sure that the control gains derived in this section satisfy the string stability criteria enforced by Equation (4.7). Figure 4.6 shows that indeed the magnitude of the complementary sensitivity stays below a magnitude of 1(0 dB) across all frequencies.

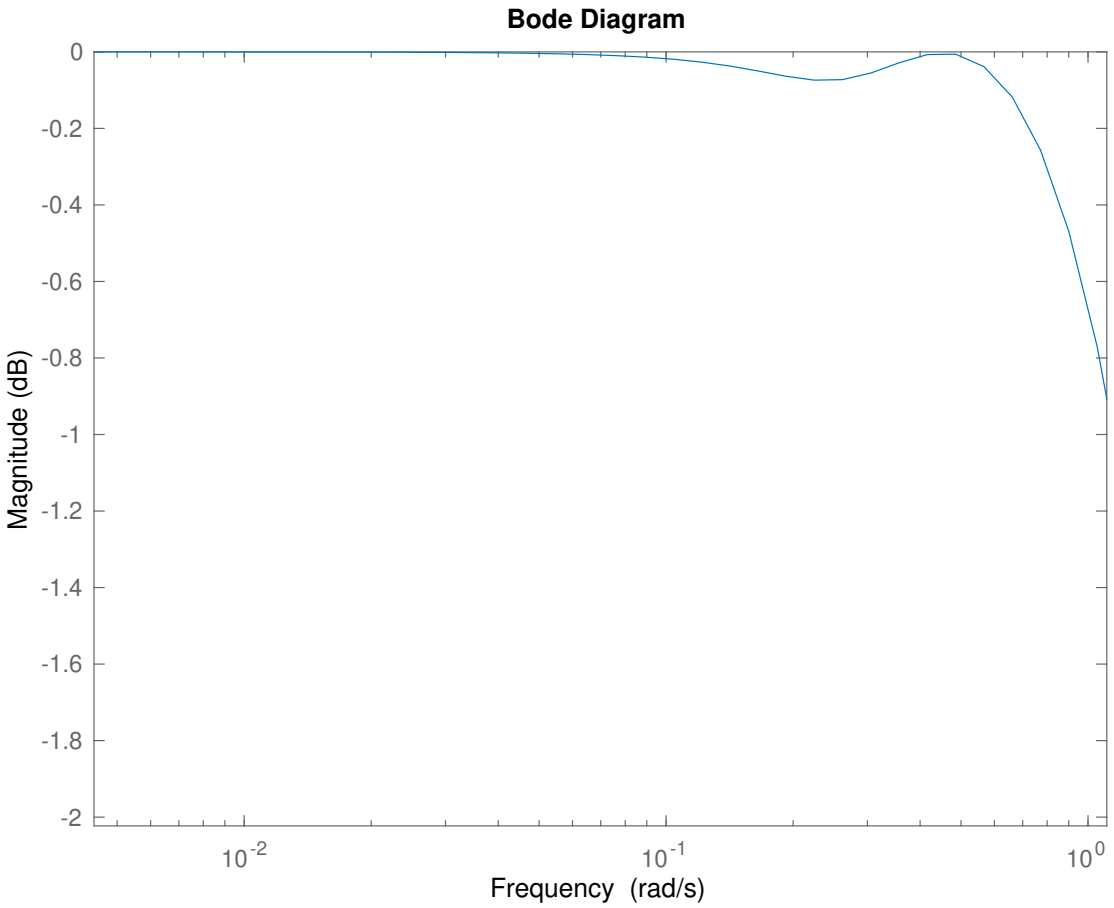

Figure 4.6: Complementary Sensitivity of the Closed loop system

Incorporating the spacing policy within the system model allows for the string stability of the platoon to easily be evaluated across several distances. By maintaining the control gains as constant and varying the time spacing, one can identify at what point the system loses its string stability properties. Figure 4.7 shows that between a time gap of .6-.4 seconds the system loses its string stability qualities for the parameters outlined in Table 4.2.

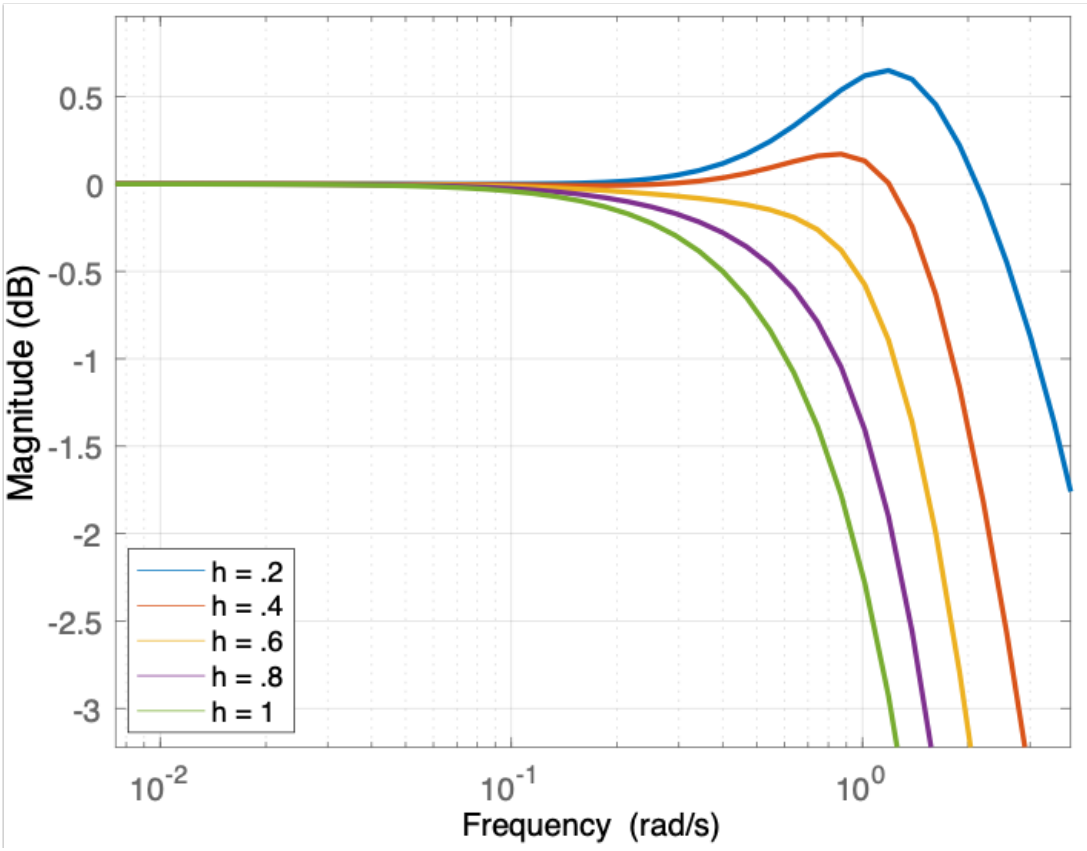

Figure 4.7: Complementary Sensitivity Over Multiple Time Gaps

4.3 Experimental Validation

It was important to validate the string stability of this system before attempting to platoon on roads with external disturbances such as grade. During this evaluation period only 3-trucks were available. The specifications of the trucks used in this testing are outlined in Table 7.2.

Table 4.3: Configuration of trucks used in the H_∞ testing

Truck	Model	Mass [kg]
Leader	2015 Peterbilt 579	32000
Follower 1	2009 M915A5	19513
Follower 2	2009 M915A5	22888

The trucks were run at the National Center for Asphalt Technologies (NCAT) test track in Opelika, AL. NCAT is a 1.7 mile long oval test track with straight that are approximately a half mile long and is shown in Figure 4.8.

Figure 4.8: NCAT Test Track

To test the string stability of the system, a "step-input" was commanded from the lead vehicle, which was manually controlled. The driver of the lead vehicle accelerated from 45MPH to 50MPH and back down to 45MPH. Figure 4.9 shows that the velocity perturbation does not results in an increasing acceleration for every vehicle down the line of the platoon. Instead the system has a decaying velocity profile, which is a clear indication that string stability has been achieved for this non-homogeneous platoon.

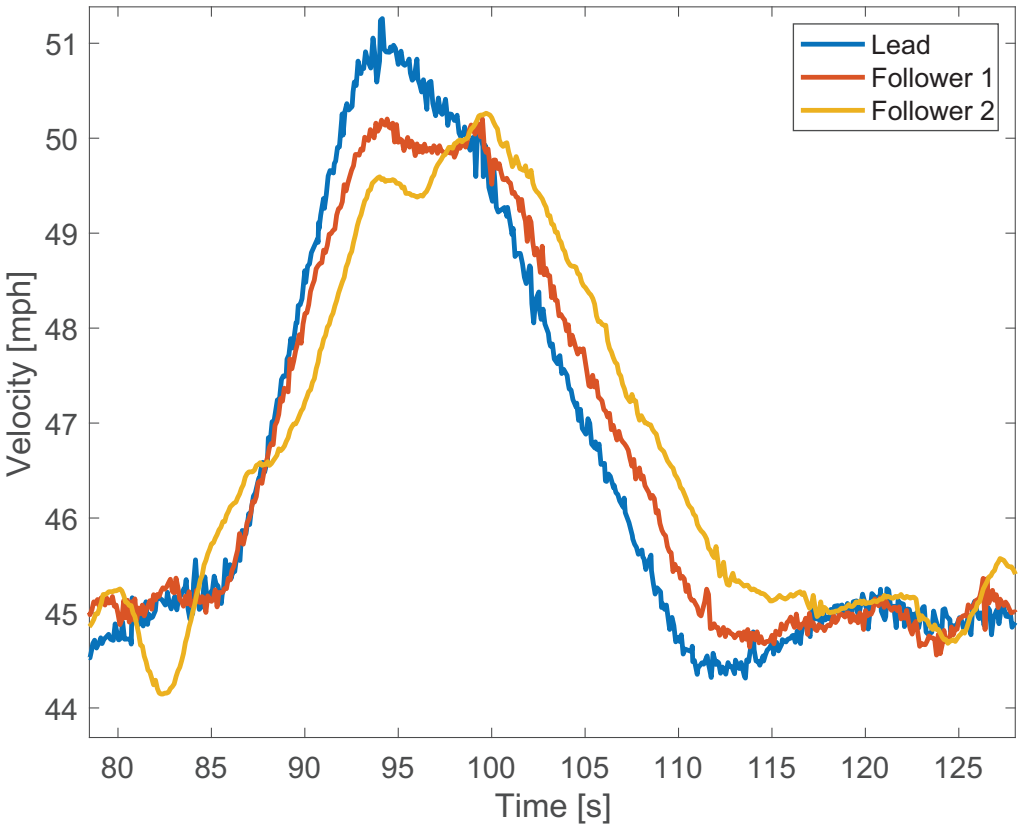

Figure 4.9: Experimental Results from a 3-Truck H_∞ platoon

Chapter 5

Nonlinear Model Predictive Control Design

Having derived the longitudinal model of the system and the terrain map has been created the Nonlinear Model Predictive Control (NMPC) controller can be developed. The goal of this model predictive controller is to develop a controller that can take into account upcoming terrain using the pre-defined terrain map and generate an optimal velocity profile that minimizes fuel consumption; all while maintaining the aerodynamic benefits of platooning. The rest of this chapter focuses on the development and implementation of a controller that achieves this goal for both the leading and following vehicle in the platoon.

5.1 Model Predictive Control Background

As the name suggests, Model Predictive Control relies on a dynamic model of a system to predict the future states of the system. MPC will then use this information to generate an optimal control output to minimize a specified objective. The dynamic model can be written generically as

$$\dot{x} = f(x, t, u) \tag{5.1}$$

where x, t and u are the current states of the system, the current time and the current control inputs to the system, respectively. These states are propagated forward through time to a future time T_f using a discrete time interval Δt. These forward predictions result in a state prediction horizon $[x_{Ti}, x_{Ti+dt}, ..., x_{Tf}]$.

There are several ways to propagate or integrate these states forward in time. One of the most common methods is Euler's method which can be written in a discrete sense as

$$x(k+1) = x(k) + \dot{x}(k) * \Delta t \tag{5.2}$$

Euler's method does rely on having a sufficiently small time step to accurately approximate any nonlinear function. This can be a major drawback as decreasing the time step while maintaining the same prediction time Tf can result in a large prediction horizon vector which can result in slow optimization times. As a results, it is desired to use an integration method that handles non-linearities better and can thus rely on a larger Δt and have a smaller prediction horizon vector.

For this reason, the Runge-Kutta 4th order method (RK4) is used as the integration method for this thesis. The RK4 integration method can be written as Equation (5.3).

$$k_1 = f(x_i, t_i) \tag{5.3a}$$

$$k_2 = f(x_i + h * \frac{k_1}{2}, t_i + \frac{h}{2}) \tag{5.3b}$$

$$k_3 = f(x_i + h * \frac{k_2}{2}, t_i + \frac{h}{2}) \tag{5.3c}$$

$$k_4 = f(x_i + h * k_3, t_i + h) \tag{5.3d}$$

$$x_{i+1} = x_i + \frac{1}{6}(k_1 + 2k_2 + 2k_3 + k4) \tag{5.3e}$$

The propagated states from Equation (5.3) could now be formulated into a cost function. However there are no constraints on any state or control variables, so the optimized output could be unrealistic. In order to make sure that certain state or control variable conditions are not violated certain equality and inequality constraints can be formulated as shown in Equations (5.4-5.5)

$$c_i(x) \geq 0 \ \ \forall \ \ i \in \mathcal{I} \tag{5.4}$$

$$c_e(x) = 0 \ \ \forall \ \ i \in \mathcal{E} \tag{5.5}$$

where $\mathcal{I}$ and $\mathcal{E}$ represent the total set of all inequality and equality constraints respectively.

Utilizing these constraints it becomes much easier to constrain the output of the system such that the control output is a usable value. One example to help in understanding this concept is that an unconstrained optimizer could request that an engine request a torque of 4000Nm which is completely unrealistic. By adding the constraint $(2300 - u_{trq} \geq 0)$, the optimizer will now only return an engine torque that is under the 2300Nm and is feasible for a class-8 vehicle. Similar constraints can also be formulated to put limits on maximum and minimum values for system states such as a maximum or minimum allowed velocity.

5.2 Lead Vehicle Optimization Setup

From the formal definition of string stability in Equation (4.7) it is shown that the acceleration of the lead vehicle impacts the rest of the platoon. In an attempt to allow for more efficient platooning it was desired to design a controller for the lead vehicle of the platoon that would be fuel-optimal over some pre-defined terrain. By implementing optimal control on the lead vehicle the affects of improved cruise-control can be singled out in future analysis. To distinguish this method of optimal cruise control from traditional cruise control, it will be referred to as eco-cruise for the remainder of the thesis.

5.2.1 Selection of System States

To begin the design of the NMPC system, the relevant vehicle states must be identified. In order to include information about terrain slope, there must be knowledge of where the vehicle is located. Additionally, it is important to be able to model the effects of the terrain on the vehicle's velocity. Therefore, the chosen system states x_1 and x_2 position and velocity, respectively. The system states and their derivatives are therefore written in matrix form as Equation (5.6)

$$\frac{d}{dt}\begin{bmatrix} x_1 \\ x_2 \end{bmatrix} = \begin{bmatrix} x_2 \\ \ddot{x}_1 \end{bmatrix} \tag{5.6}$$

where $\ddot{x}_1$ is the vehicle acceleration which was previously defined as Equation (2.1).

5.2.2 Selection of Prediction and Control Horizon Parameters

Now that the states for the model have been defined, the next step is determining the prediction and control horizons. Most resources in optimal control have chosen look ahead distances of greater than a mile [14, 16] because prior research has shown that the average slope length of a crest or sag is less than 3000m in length [26]. Since data had already been collected to build a terrain map such as the one outlined in chapter 3, all information pertaining to hills was already known. Therefore a half hill analysis was performed against the national activity-weighted average half hill statistics presented in [27] where a half hill is defined as a section of road where the road grade does not change sign. Figure 5.1 presents the comparison of the highway-280 half-hill data to the national data.

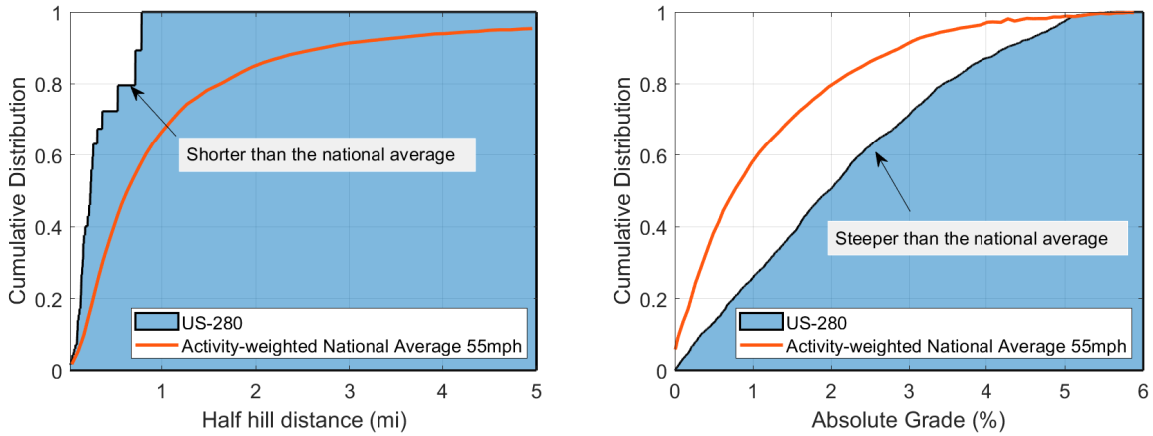

Figure 5.1: Eastbound test section grade characteristics versus 55mph activity-weighted national average [17]

It can be seen that the highway-280 test has both shorter and steeper hills than the national average. The half hill analysis also revelaed that all hills on the test route can be captured within a 1500m look ahead distance. Therefore, a 1500m look ahead distance was selected

rather than the more common 3Km look ahead distance. Table 5.1 summarizes the design choices for the discretization of the system states.

Table 5.1: Discretization Options for Lead Vehicle O.C.

Look ahead Distance	1500m
Discretization Length	25m
Prediction Horizon Length	N = 60
Control Horizon Length	N = 60

5.2.3 System Constraints

One of the shortcomings mentioned about classical control methods is their lack of knowledge of system constraints. Therefore it was desired to include system constraints into the optimization so that a realizable control actuation output is generated.

One of the more prominent constraints to be included is the maximum allowable engine torque for the vehicle. Because of how the optimal control problem is formulated in code and how the 3-link fuel rate model is defined, an explicit constraint on the peak output torque is not necessary. To understand why, recall that the maximum engine torque is only a function of the vehicle wheel speed, as previously discussed in Chapter 2.

Fuel consumption is only a function of the actual engine output torque and the current engine RPM. Both of these relationships are defined previously by Equations (2.7) and (2.9). Since the maximum torque at any given RPM is represented by a polynomial function, it is impossible to command an output torque larger than the maximum value of the polynomial so long as $u_{throttle}$ remains less than or equal to 1. Therefore the only inequality constraints added to the system are on the value of $u_{throttle}$ and the minimum value of the braking torque which is defined separately from the engine torque. These constraints are written as Equations (5.7) and (5.8), respectively.

$$0.0 \leq u_{throttle} \leq 1.0 \tag{5.7}$$

$$\tau_{brake} \geq -3000 \tag{5.8}$$

5.2.4 Cost Function

Defining the cost function is important for several reasons. The first reason is that the cost function dictates what the system is trying to optimize. Secondly, the weighting of the terms within the cost function play a key role in deciding system response parameters such as overshoot and settle time. If the system were only trying to minimize fuel consumption the truck would never move as the most fuel optimal thing it could do is to remain static. Therefore the cost function was defined as Equation (5.9)

$$J_{eco-cruise} = Q_1 \sum Err_{vel}^2 + Q_2 \sum fuel_{consumed}^2 \tag{5.9}$$

where the velocity error term is included to make sure the system will track a desired velocity.

Equation (5.9) has two distinct weights internal to the problem that can be tuned to achieve the desired optimal performance which are Q_1 and Q_2. If Q_1 were zero, the system would slowly coast to a stop because the most fuel-optimal thing to do would be to not drive. Conversely if Q_2 were zero the system would aggressively try to track the reference velocity over the given terrain. The final selection of the weights for the cost function and evaluation of this optimizer will be covered in a later chapter.

5.3 Following Vehicle Optimization Setup

The following vehicle optimization is similar to eco-cruise in how several of its states are defined. However, a key difference is that rather than trying to balance the platform velocity with fuel economy, the following platform tries to balance the inter-vehicle spacing, or headway, with fuel economy. Figure 5.2 provides an overview of the leader-follower platooning scenario where h_{ref} and h are the reference heading and actual heading, respectively. The

remainder of this section will outline the exact system states and system parameters used for the configuration of the optimal-following controller.

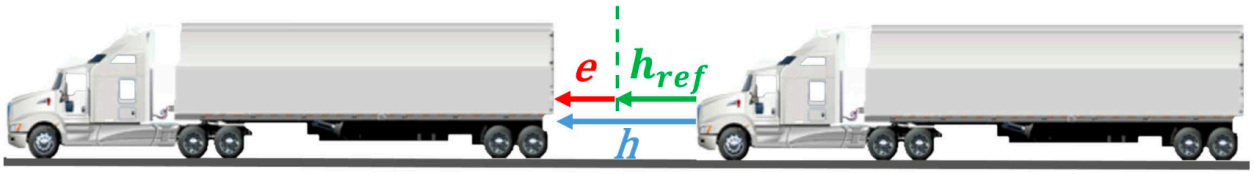

Figure 5.2: Leader-Follower Platooning Diagram [23]

5.3.1 Selection of System States

For the following vehicle, the headway between the two platooning vehicles is the most safety critical parameter and also the most critical in generating aerodynamic fuel savings. Additionally, it is not possible to generalize the behavior of both the lead and following vehicle over a 1500m interval. This means that trying to balance optimal fuel-economy with maintaining a nominal headway would be increasingly unreliable further into the prediction horizon, and the computational complexity would also increase. Therefore it was decided to focus only on the short term dynamics that occur between the vehicles.

Additionally, it is common that in many similar works that the optimal control problem be converted from the time domain to the spatial domain using the relationship expressed in Equation (5.10).

$$dt = \frac{1}{v} dp \tag{5.10}$$

However in this thesis it was decided to leave the optimal control formulation in the time domain. The justification for leaving the problem in time domain comes from the discussion on the impact of map mismatch in chapter 3. Chapter 3 says that as long as the magnitude in grade is correct, position error on the map has a relatively small impact on the output of the optimal control solution. This is because a few meters of position error is relatively

small on the scale of hills with inclines and declines that are on the order of 100's of meters. Therefore any mismatch in assigning grade at each time step should be of minimal impact.

Since the code that provides the discrete grade profile to the optimizer runs as an independent software process, the optimal following code can ignore the global position variable and instead focus only on the inter-vehicle headway, the lead vehicle's velocity and the following vehicle's velocity. These states and their derivatives are defined by

$$\frac{d}{dt}\begin{bmatrix} v_{i+1} \\ v_i \\ \Delta x \end{bmatrix} = \begin{bmatrix} e^{-2t} * \dot{v}_{i-1} \\ \dot{v}_i \\ v_{i+1} - v_i \end{bmatrix} \tag{5.11}$$

where v_i denotes the velocity of the following vehicle and v_{i+1} denotes the velocity of the preceding vehicle. Since both vehicles are equipped with Dedicated Short Range Communication (DSRC) radios, the following vehicle is able to receive the acceleration of the preceding vehicle. It uses this information to apply a first order decay to that acceleration and generate an estimated velocity profile for the leading vehicle.

5.3.2 Selection of Prediction and Control Horizon Parameters

Selection of the prediction and control horizon parameters for the optimal-following algorithm is much more arbitrary than the previously described eco-cruise parameters. This is mainly because the parameters can vary greatly depending on what the control engineer values most. For example, if the computation time of optimizer is of little concern, then it is best to increase the look-ahead time for the optimal follower. This is due to the fact that a further look-ahead time will allow the optimizer to capture more of the upcoming grade. The downside to increasing the look-ahead time is that the accuracy of the projected headway will decay with the increased look-ahead time which could cause the optimal velocity profile to change. For this thesis, a faster run time was desired so the look ahead time is short

compared with the equivalent look ahead time of eco-cruise. Table 5.2 presents the relevant discretization options used for the optimal follower.

Table 5.2: Discretization Options for Follower Vehicle O.C.

Look Ahead Time	4s
Control Horizon Length	N = 60
Control Horizon Length	N = 60

5.3.3 System Constraints

Optimal following is very similar to eco-cruise in the aspect that they're both optimizing a velocity profile through the usage of the "3-link" fuel-rate model. Therefore, the same constraints placed on the normalized throttle and braking torque applied to eco-cruise in Equations (5.7 - 5.8) are also applied to the optimal following controller.

In addition to the constraints on the driveline, there are now additional safety constraints that should be considered. If no limits are placed on the allowable headway, it is possible that the vehicle could request a dangerously close headway. While this would certainly be great from an air-drag reduction perspective, the risk would just be too great for a real world application. Therefore a closest minimum headway must be implemented. In this case a minimum headway of 25 feet, or 7.62 meters, was chosen and is written as Equation (5.12).

$$headway - 7.62 \geq 0.0 \tag{5.12}$$

5.3.4 Cost Function

The cost function should always be indicative of the overall objective of the platooning vehicle. In this case the objective of the platooning vehicle is to optimize fuel economy while minimizing headway errors. Therefore a baseline cost function should take the shape of Equation (5.13)

$$J_{eco-cruise} = Q_1 \sum hdwy_{err}^2 + Q_2 \sum fuel_{consumed}^2 \tag{5.13}$$

In this thesis it is also desired to penalize the relative velocity between the leader-follower vehicles, called the headway-rate. The first reason for this is to prevent an unsafe scenario in which the following vehicle closes any growth in the headway error too quickly, creating an unsafe scenario. The goal in penalizing the headway-rate is to limit unnecessary braking and the wasting of energy by the follower vehicle. Therefore the final form of the cost function for the optimal-following vehicle is Equation (5.14)

$$J_{eco-cruise} = Q_1 \sum hdwy_{err}^2 + Q_2 \sum fuel_{consumed}^2 + Q_3 \sum \dot{hdwy} \tag{5.14}$$

5.4 Real-Time NMPC Implementation

For NMPC systems, there is often another set of design considerations that need to be made. These design considerations mainly take the form of deciding what the actual implementation of the controller should look like. There are always several trade offs to be made in terms of simplicity and ease of implementation. Additionally, the specific way in which the controller is implemented can often be informed by the trade-offs selected in the software implementation of the system.

In some recent state-of-the-art works such as [16, 28] a unique centralized/de-centralized control approach is taken. This is achieved by splitting the optimal-control problem into two different layers called the platoon layer and vehicle layer. The platoon layer specifically handles the generation of a fuel-optimal speed profile for the entire platoon while satisfying an average speed requirement provided by the fleet layer. The fleet layer in this case determines the optimal route to get to from the platooning start location to the platoon ending location. The vehicle is responsible for the real-time vehicle control. Every vehicle has its own vehicle

layer that will track both the desired speed and gap distance but also guarantees safety by preventing collisions. An overview of this control architecture can be seen in Figure 5.3.

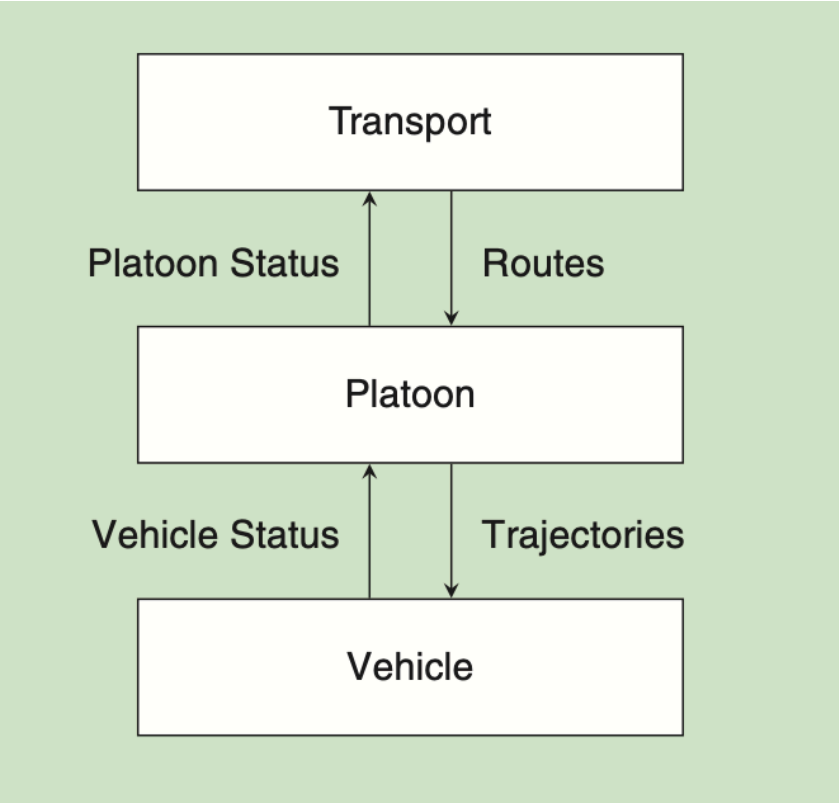

Figure 5.3: Layered Transportation System Architecture [28]

While this is certainly an effective approach it does assume that all layers of the system have access to information about all the vehicles in the platoon. Additionally it then becomes prohibitive for other trucks on the road to join a platoon. To make this system as generic as possible there is no assumed transport layer optimizing the vehicle route and the responsibilities of the platoon layer are handled by each individual vehicle at the vehicle layer.

The main benefit to this approach is that no vehicle in the platoon needs knowledge of the mass, gearing or engine information of any other vehicle in the platoon. This allows for every vehicle to optimize its velocity profile individually. By adding in the constraints such as minimum following distance, every vehicle is also responsible for maintaining a safe distance from other vehicles in the platoon. While V2V communication certainly helps the

system in predicting the states of the other vehicles in the system it is not required. This prevents issues where perhaps different vehicles running different versions of the software could not enter the platoon.

One thing all of the works in this field do recognize though is the computational complexity of the NMPC algorithm. By using the layered approach the computation time is abstracted to a layer that doesn't affect the vehicle controller. In other works such as [14] the controller is generating the reference velocity and controller commands. When generating both the reference velocity and commanded torque the optimization time is typically between 1-5Hz. At 1-5Hz any emergency maneuvers or fast dynamics would be lost. Therefore a lower level velocity controller is needed. This thesis utilized a lower level PID velocity controller that takes the reference velocity from the optimizer and generates a torque to regulate the vehicle velocity do the desired reference at a 20Hz. Figure 5.4 displays the control architecture used in the remainder of this work.

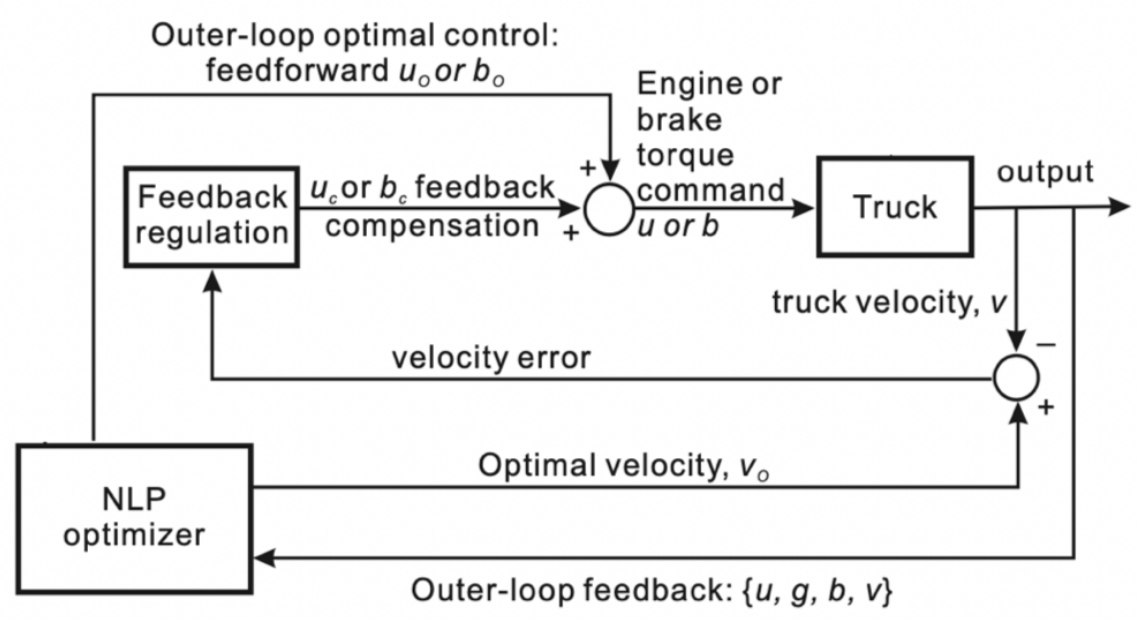

Figure 5.4: Nested NMPC Control Architecture [14]

Chapter 6

NMPC Platooning Simulation Results

In research that require time-intensive testing to evaluate the efficacy of the control solution, performing all testing and troubleshooting in the real-world is not a tractable or cost-effective solution. In order to tune the control system and test various cost functions a simulation environment is needed. TruckSim is a high fidelity vehicle modeling and simulation tool used across academia and industry to help reduce cost of vehicle prototyping and testing Advanced Driver Assistance Systems (ADAS) systems [29, 30]. In prior research such as [23] a two-truck class-8 vehicle platoon was simulated going over uneven terrain. This thesis takes the same simulation environment tested in [23] and updated the terrain profiles and control scheme. Eco-cruise was evaluated extensively in TruckSim with results presented in this chapter. Unfortunately due to internal solver errors encountered in Simulink and the time restrictions imposed by vehicle and personnel availability, optimal-following was unable to be extensively tested in TruckSim.

6.1 Simulation Scenarios

Simulation is a key tool in tuning a NMPC cost function. By sweeping the cost function weights over some set of numbers. By comparing the final cost function value and system behavior for each set of weights an ideal cost function can be found. To aid in determining what acceptable behavior was it was decided to reference simulation results from [14] as a comparison for the eco-cruise controller.

Two key scenarios to evaluate the controller on are on the approach and climb of a linear incline and decline. Figure 6.1 represents the first test scenario that the eco-cruise algorithm will be evaluated against. This figure presents both the Optimal Control (O.C.)

velocity profile and the velocity profile of the traditional cruise-control algorithm. Figure 6.1 provides great insight about the difference between an optimal controller versus a traditional controller. The primary difference is that it is desired to accelerate before encountering grade, and then allowing a gradual deceleration on the hill. This avoids a downshift and higher engine RPM where engine efficiency is greatly reduced.

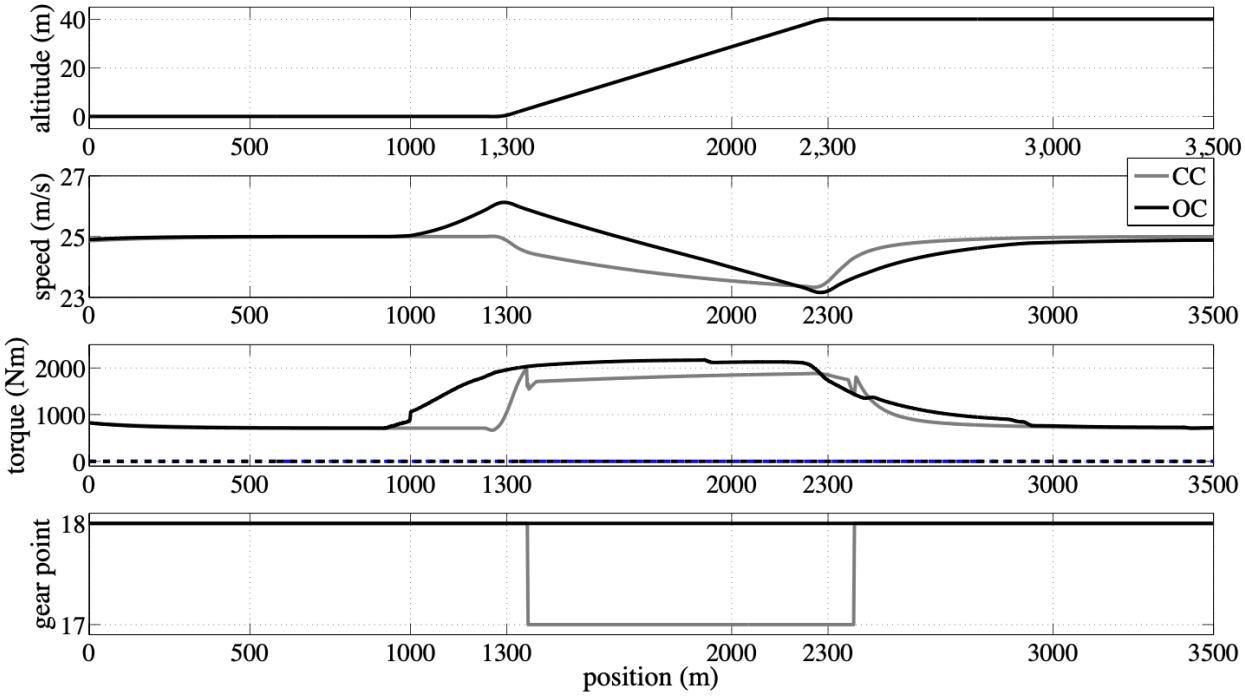

Figure 6.1: Uphill Optimal vs Traditional Results from [14]

After a few rounds of tuning, the Eco-cruise results were able to accurately represent the results found in Figure 6.1. The weights for the cost function were set and logged in Table 6.1. While it seems counter-intuitive to weight the fuel consumed less than the velocity error, it is important to remember the the units and therefore the magnitude of the two terms in the cost function are drastically different. The ratio between the two terms in the cost function is what is really important and Figure 6.2 matches the desired performance.

Due to poor optimization run-time, the eco-cruise controller was set to run only at 2Hz and execute a zero-order-hold (ZOH) for all time-steps in between. This results in the torque command seen in the figure. Figure 6.2 shows that the designed eco-cruise system

Table 6.1: Eco-Cruise Cost Weightings

Cost function Term	Weighting Value
Vel_{err}	$\text{Q}_1 = 10$
$\int \dot{Fuel}$	$\text{Q}_2 = 1$

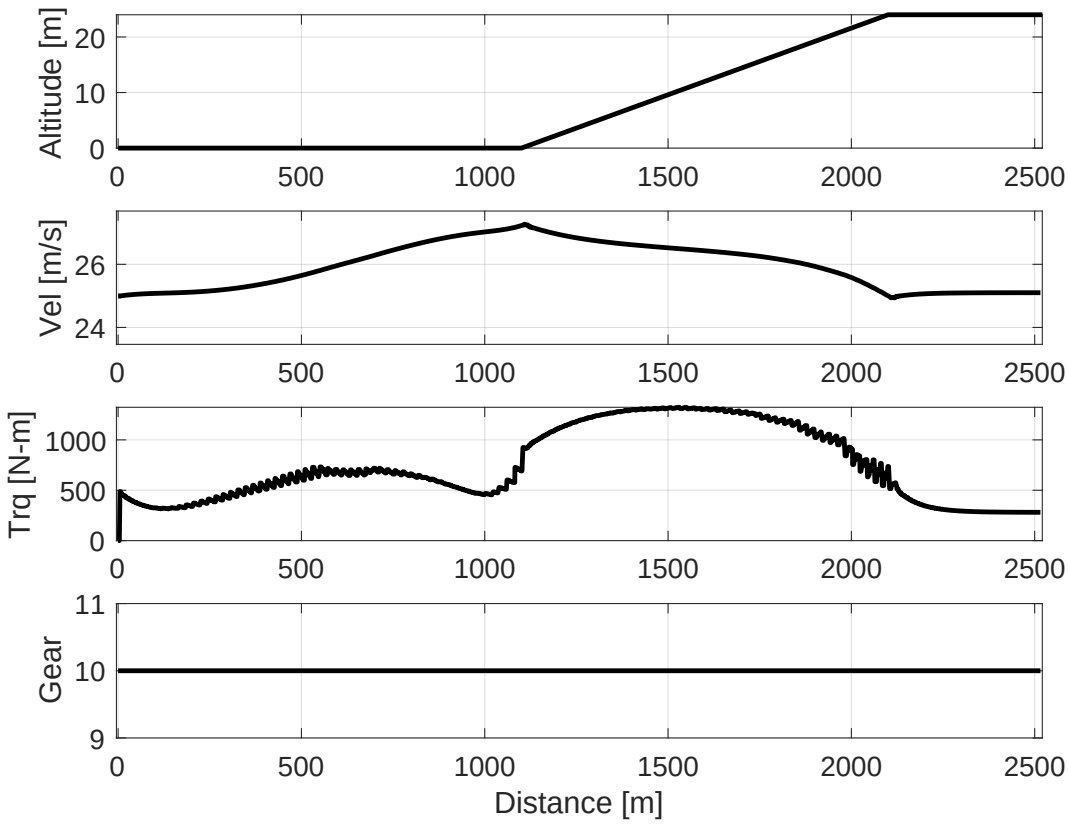

Figure 6.2: Eco-Cruise Uphill Test in TruckSim Using Values from Table 6.1

does in fact increase the vehicle velocity prior to hitting the hill, and allows the vehicle to gradually slow back down to the target velocity. It is also important to note that the system avoids shifting gears during this event. No fuel results are presented in this section due to the extreme simplicity of the fuel-rate and engine model implemented in this TruckSim configuration.

The next test is the down hill driving test. Figure 6.3 presents the results from [14] which compares the optimal control performance against the traditional cruise-control performance. The key takeaway from this plot is that it's desired for the vehicle to reduce its velocity before

cresting the hill and allowing the conversion from potential to kinetic energy to speed the vehicle back up to the desired velocity.

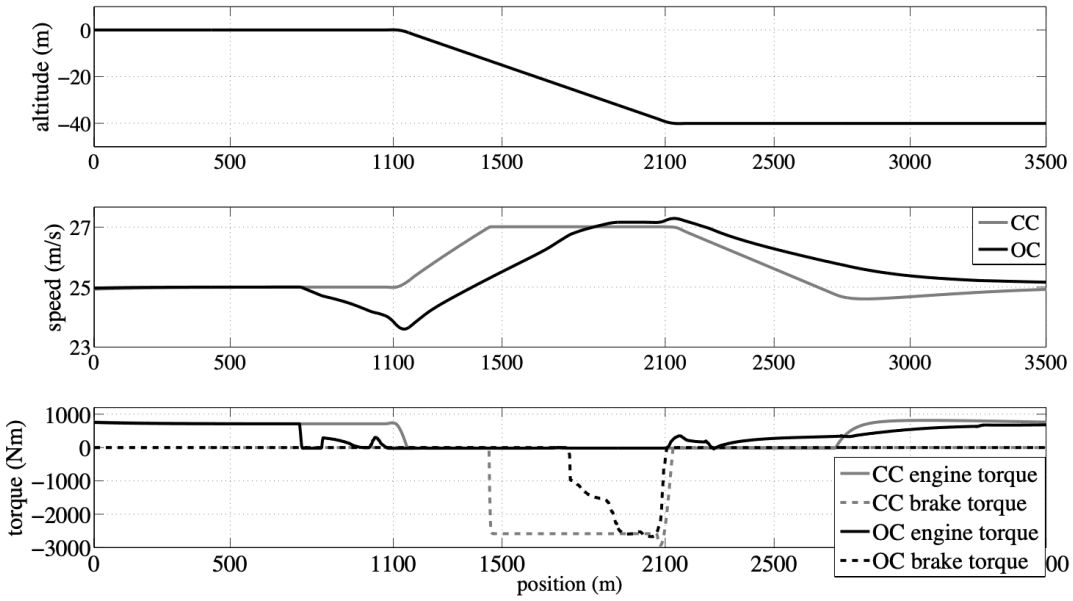

Figure 6.3: Downhill Optimal vs Traditional Results from [14]

Figure 6.4 uses the same controller weightings from Table 6.1 to simulate the eco-cruise controller going downhill. Again it can be see that the controller designed in this thesis is able to successfully replicate the results from [14] by allowing the vehicle to slow down before cresting the hill.

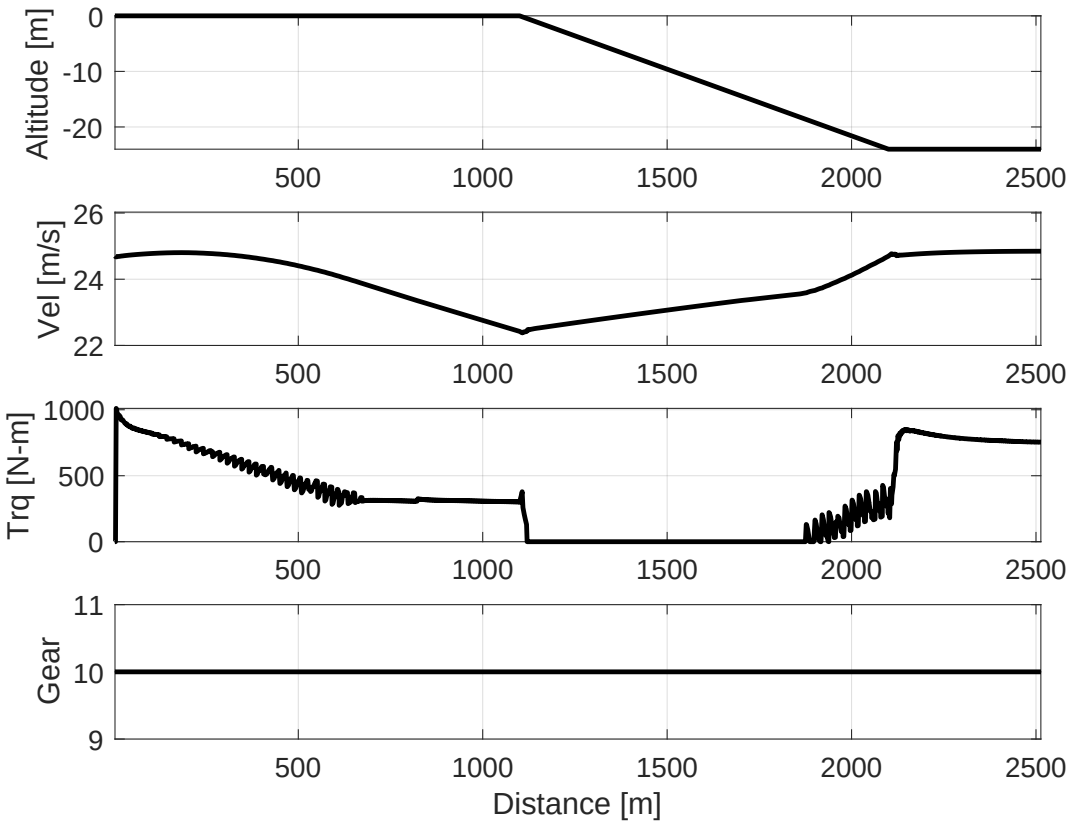

Figure 6.4: Downhill Eco-Cruise Results

6.2 Optimal Follower

It was also strongly desired to simulate the full system dynamics of a two-truck optimal platoon in simulation before implementing the real-time software on a commercial vehicle. However, after implementing the software into the same TruckSim/Simulink system as eco-cruise, MATLAB would return "linesearch" and various other optimization errors. These errors were not able to be resolved in a timely manner before first round fuel-testing was to begin. However, it is still important to have some level of confidence in the performance of the optimal following software before allowing it to run on a commercial vehicle.

To generate appropriate first-pass controller gains and have confidence in the software, a different approach had to be developed. In order to do this, a two-truck platoon was run on the desired test loop of highway-280 with both truck transmitting and recording all sensor and radio data. The trucks drove in such a way that most common platooning scenarios

would be captured. These scenarios included gaining on the lead-vehicle while approaching a hill, falling back while approaching a hill and several steady-state platooning scenarios.

By taking advantage of the rosbag play feature, this data was able to be run through the C++ implementation of the optimal-follower software. After addressing any software bugs, the commanded control signal and predicted inter-vehicle spacing was examined. This method yielded the initial optimization weights that were used for the first test run on highway-280. These control gains are listed out in Table 6.2

Table 6.2: Optimal-Follower Cost Weightings

Cost function Term	Weighting Value
hdwy_{err}	$Q_1 = 5$
hdwy_{rate}	$Q_2 = 1$
$\int Fuel$	$Q_3 = 5$

Chapter 7

Experimental Results

7.1 Experimental Test Planning

The testing in this section was designed in the spirit of the SAE J1321 Type-II fuel testing standard [31]. This standard describes a procedure to eliminate as many external variable from the fuel results as possible. Again, due to time and financial constraints, not all of these procedures were able to be followed. Table 7.1 lists several of the Ypye-2 processes and shows if this thesis met the specific process or not. It is important to note that this table is NOT inclusive of all SAE type-II fuel testing procedures.

Table 7.1: Overview of Type-2 Testing Procedures

Type-II Procedure	Satisfied in Testing
1-Hour vehicle warmup	YES
Stop time $<$ 30% of test time	YES
Control vehicle running $>$ 1500ft. behind platoon	YES
Calibrated high-precision fuel-flow meter (not gravimetric)	YES
Mean wind speed $<$ 12mph	YES
Locked A/C settings	YES
1-Hour or 50-mile test route	NO
Control vehicle same as platooning vehicle	NO

To classify any fuel savings as type-II fuel results as statistically relevant, a given test configuration must have 3 allowable test runs. Some test runs may be a statistical outlier which would then rejected. For this reason, not all test runs were used in the final analysis. Due to the time and personnel constraints, replicate runs were not able to be run. Later sections will detail the exact number of runs every platooning configuration was able to successfully run.

Table 7.2 outlines the vehicles used in this testing. It was desired to have the most power-limited vehicle serve as the lead-vehicle in this platoon. While both testing vehicles are the same, the control vehicle as noted in Table 7.1. This is of relatively little impact for the final fuel results because of how the fuel-savings are calculated. The purpose of the control vehicle is mainly to allow a way to capture the impact of external influences such as road temperature, air temperature, and wind in the reference measurement.

Table 7.2: Configuration of trucks used in the Type-II testing

Truck	Model	Mass [kg]
Leader (eco-cruise)	2009 M915A5	22888
Follower (optimal-following)	2009 M915A5	19513
Control (cruise-control)	2015 Peterbilt 579	32000

A 15.4 mi (24.8 km) loop on highway US-280 was selected as the test section for this testing. For consistent analysis,the data was bounded to constant velocity portions of the test loop for all runs, approximately 8 km on both the east- and westbound segments. This thesis only analyzed the impacts of the Eastbound map however as the Westbound track is flat and will not give much insight into the benefits of optimal platooning. Figure 7.1 shows the total test route driven with the green portion representing the eastbound segment.

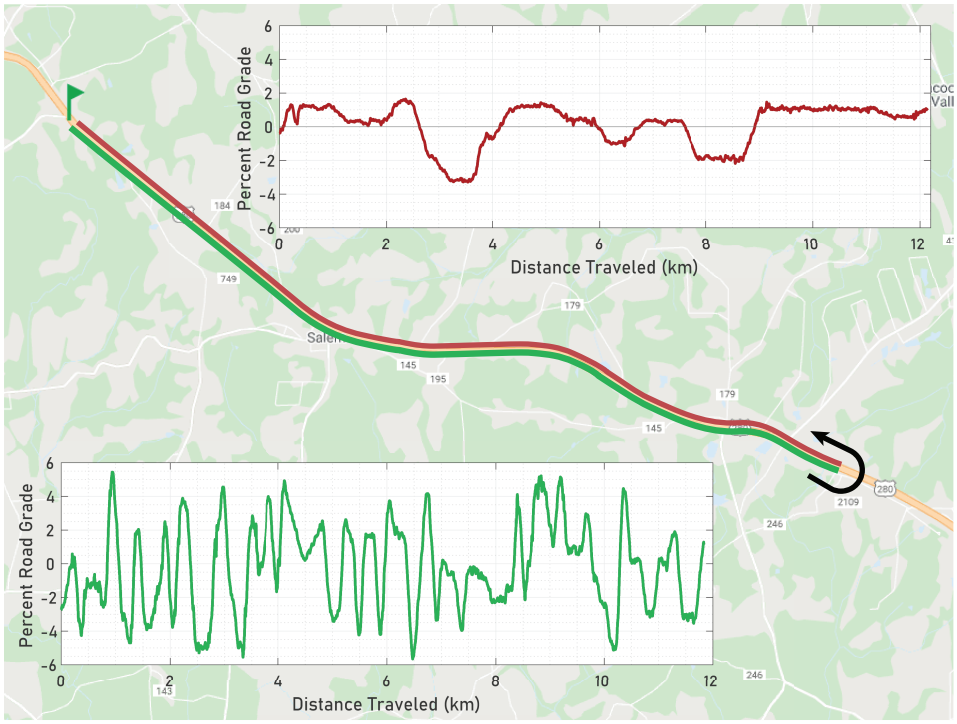

Figure 7.1: Experimental Testing Test route (Eastbound shown in green, Westbound in red) [17]

The experimental testing was limited to the 12th and 13th of June 2021. To ensure that the wind and weather constraints discussed in Table 7.1 were satisfied in this testing, weather measurements were taken from the KALSALEM weather station located approximately a half mile from the turnaround point indicated on Figure 7.1.

Since the experiments were conducted on real roads, surrounding traffic could not be controlled. The results assume that the influence of surrounding traffic on fuel consumption was a relatively constant throughout the course of the tests. No significant qualitative difference in traffic density or flow was observed by the testing personnel, and because the set speed of 55 mph is below the posted speed limit of 65 mph, there were no attempts by drivers to cut in to the platoon. The influence of surrounding traffic on a two-truck platoon was investigated in depth in [32], which found that dynamic passing events had a small impact on lead truck consumption, but not on the follower. Additionally, the experiments were all run in the platoon configuration outlined in Table 7.2 with a spacing of 36.87 meters,

or 1.5 seconds. This distance is close enough for the follower to still receive aerodynamic benefits from platooning where the leader sees little to no benefit [11].

7.2 Test Matrix

The goal of developing the test matrix was to ensure that any differences in the optimal versus traditional, referred to as fixed headway platooning, would be captured. Additionally, it is also important to identify any impacts that the behavior of the lead vehicle will have on the remainder of the platoon. For this reason there were four main tests that were desired to be seen with the configurations listed in Table 7.3. For brevity, tests will be referred to in an abbreviated format in future sections using ec-opt for a two truck platoon in a Eco-Cruise and Optimal-Following scenario, shown in Table reftab:testConfigurations.

Table 7.3: Experimental Testing Configurations

Leader Configuration	Follower Configuration
Cruise Control	Fixed Headway
Eco-Cruise	Fixed-Headway
Cruise Control	Optimal Following
Eco-Cruise	Optimal Following

7.3 Comparison of Run Times

One of the biggest considerations when comparing new platooning strategies is the evaluation of the run-time of the platoon. It would be easy for a platoon to conserve fuel by driving at a slower and more economical speed, however this is not a realistic option. Many drivers in industry are either paid by the mile or paid by the delivery. Therefore, creating a system which only saves fuel by going slower would immediately be rejected by trucking fleets. For these reasons, it was desired to make sure that this eco-cruise and optimal-following technology does not drastically change the drive time of the route.

Figure 7.2 presents the run-time for each of the four main configuration plus a baseline run in which the lead vehicle ran a traditional cruise-control independent of a platoon. All of the runs were within 1% of the mean run time for all westbound runs. Furthermore, all Eco-Cruise runs were faster than the cruise-control runs.

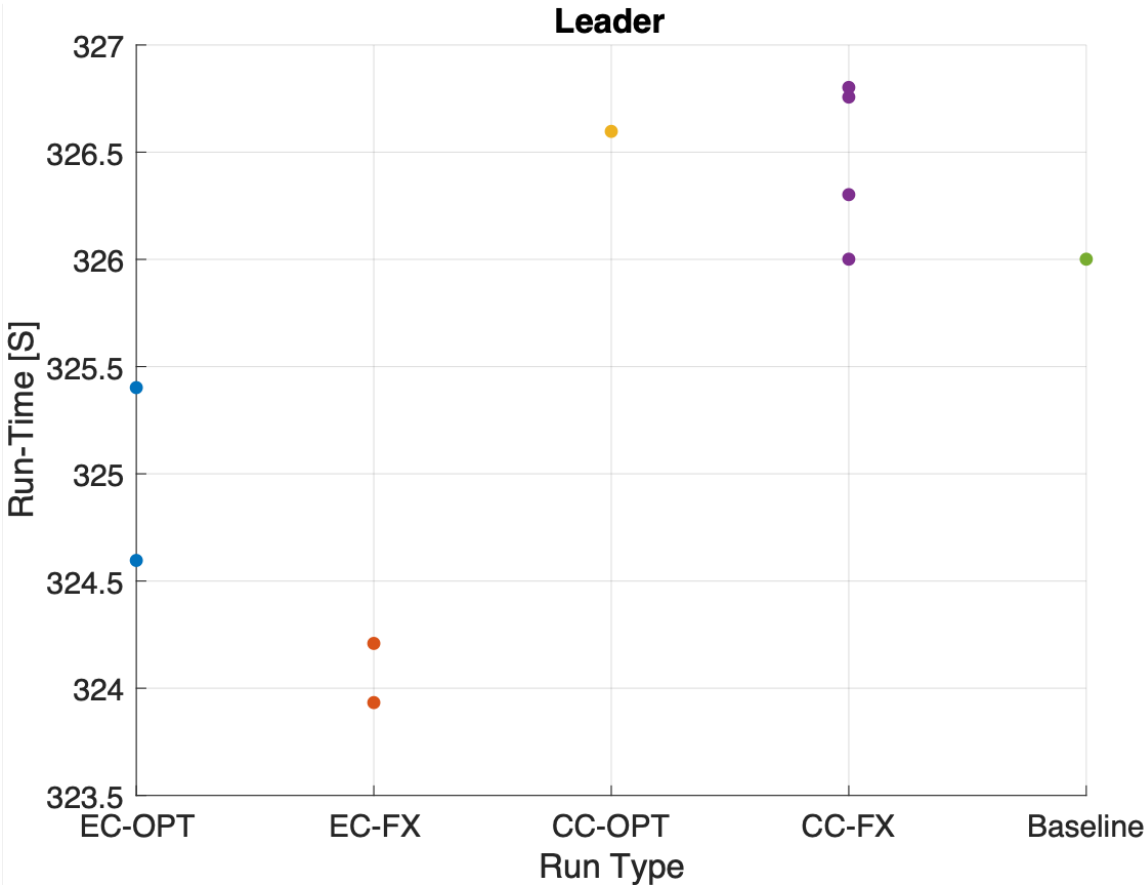

Figure 7.2: Comparison of Run Times for all Test Configurations

7.4 Method for Processing fuel Results

Before presenting the fuel-savings results, it is important to discuss the method of measuring the fuel savings. The SAE J1321 standard [31] specifies a statistical significance method for identifying fuel savings. The first step in calculating any fuel savings is to generate the ratio of the test vehicles fuel consumption to the control vehicles fuel consumption. This ratio is commonly denoted as the T/C ratio. This T/C ratio is then compared to the T/C

ratio from the other testing configuration. For example, to view the benefit of Eco-Cruise to cruise-control the two T/C ratio's to be compared would be a Eco-Cruise/Control to Cruise-Control/Control comparison. A more detailed explanation of the T/C comparison procedure is borrowed from [17]:

- Obtain T/C ratios by dividing the fuel consumption for the truck in question by the fuel control vehicle consumption for every test segment

$$T/C_{i,j} = \frac{Test\,Vehicle\,Consumption_j}{Control\,Vehicle\,Consumption_j} \text{for configuration } i \tag{7.1}$$

  where i denotes a different configuration of test, e.g. EcoCruise leader with a follower using NMPC, and j denotes the iteration number of the test.

- Select two sets of tests from i for compararison, calling one the **Baseline** and the other the **Test**.

- Compare the T/C variances between the j iterations of the **Baseline** and **Test** sets using an F test with a significance level of 0.95.

- If the variances are equal for the **Baseline** and **Test** T/C ratios, compare the T/C ratios and calculate the 95% two-sided confidence intervals of the **Baseline** and **Test** sets using a t-test for equal variances. If the vriances are not equal, use a t-test for unequal variances. This significance level is also selected to be 0.95.

- Depending on the result of the t-test (specifically, its p-value), the difference in mean T/C for the **Test** and the **Baseline** is deemed either significant or insignificant. Results are expressed as a percent improvement over the baseline ± the two-sided confidence interval.

This methodology was used to calculate the fuel results presented in all future sections.

7.5 Fuel Results

This section aims to analyze the fuel results for both the eco-cruise and optimal-follower platooning system. The analysis in this section presents both the SAE-J1321 results as well as graphical results. The combination of these two methods aims to provide an in-depth look at how the optimal platooning approaches creates a reduction in fuel savings for both optimal control methods. For a table of all fuel testing data please reference Appendix A.

7.5.1 Eco-Cruise Results

Using the provided template that comes with the SAE-J1321 standard, the Eco-cruise system was shown to save 14.1 $\pm$3.1% in fuel economy for each run. Figure 7.3 shows the mean fuel consumed by each test configuration with the number indicating the number of viable runs used to calculate the mean. One important note is that since the main comparison here is between Eco-Cruise and traditional cruise-control, runs from both EC-OPT and EC-FX can be used in the SAE-J1321 spreadsheet. This allows the fuel result calculated to meet the 3-run criteria needed to call a fuel-results significant.

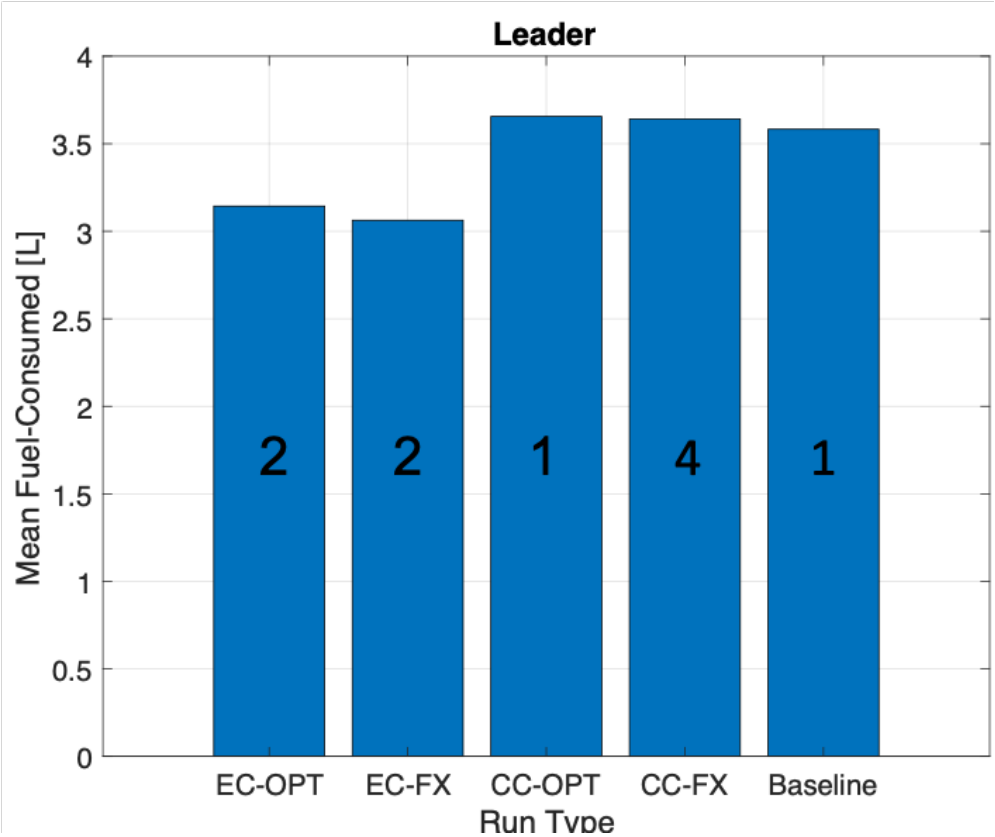

Figure 7.3: Fuel Results for the Lead Vehicle

Insight into the inefficiencies of traditional cruise-control driving can be seen by analyzing the lead truck velocity profile. Figure 7.4 showcases two of the cruise-control runs. Evaluated on a criteria of velocity regulation, this controller performs well by maintaining a vehicle velocity to within $\pm$ 1mph across most of the trip.

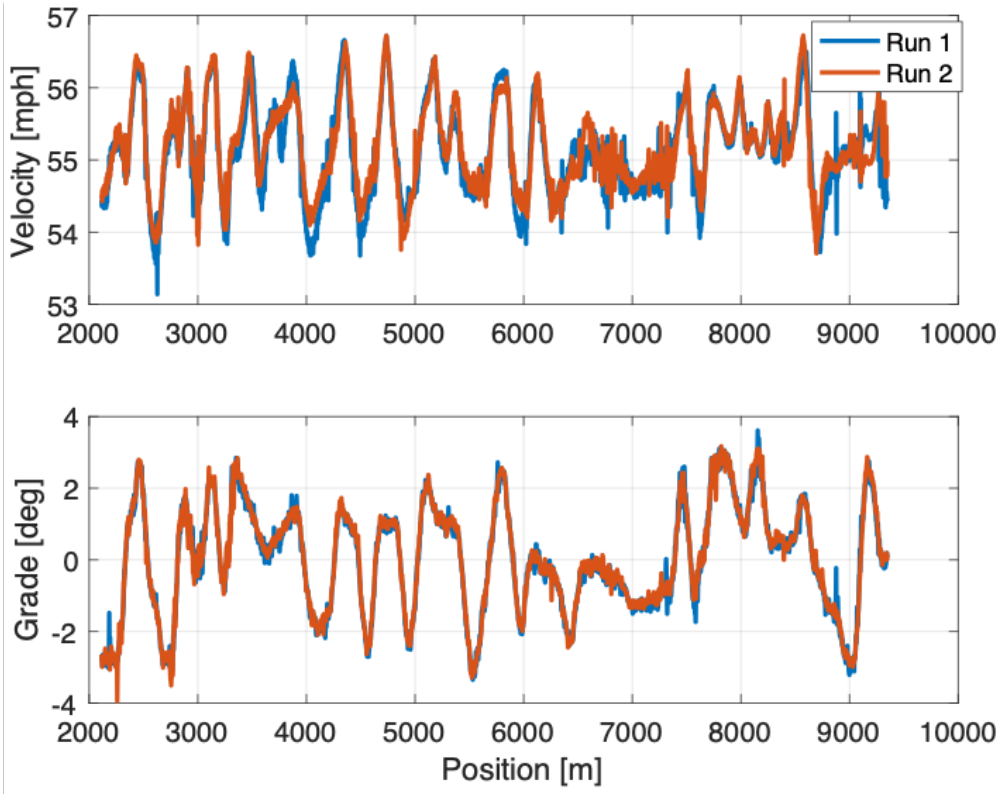

Figure 7.4: Traditional Cruise-Control on Highway-280 Test Route

When looking at a region of interest on Figure 7.4 between kilometers 4-5.5, Figure 7.5 shows the trends that may cause this method to be less efficient than an optimal method. Figure 7.5 displays that in order to regulate the vehicle velocity about the desired speed, the system would sometimes slow down on downhill areas and increase the velocity on uphill segments. By not allowing the trucks potential energy to be converted to kinetic energy on a downhill segment the truck is losing energy that could have been used to climb on the following incline. Additionally, accelerating uphill in a fully loaded class-8 vehicle is an extremely energy intensive process.

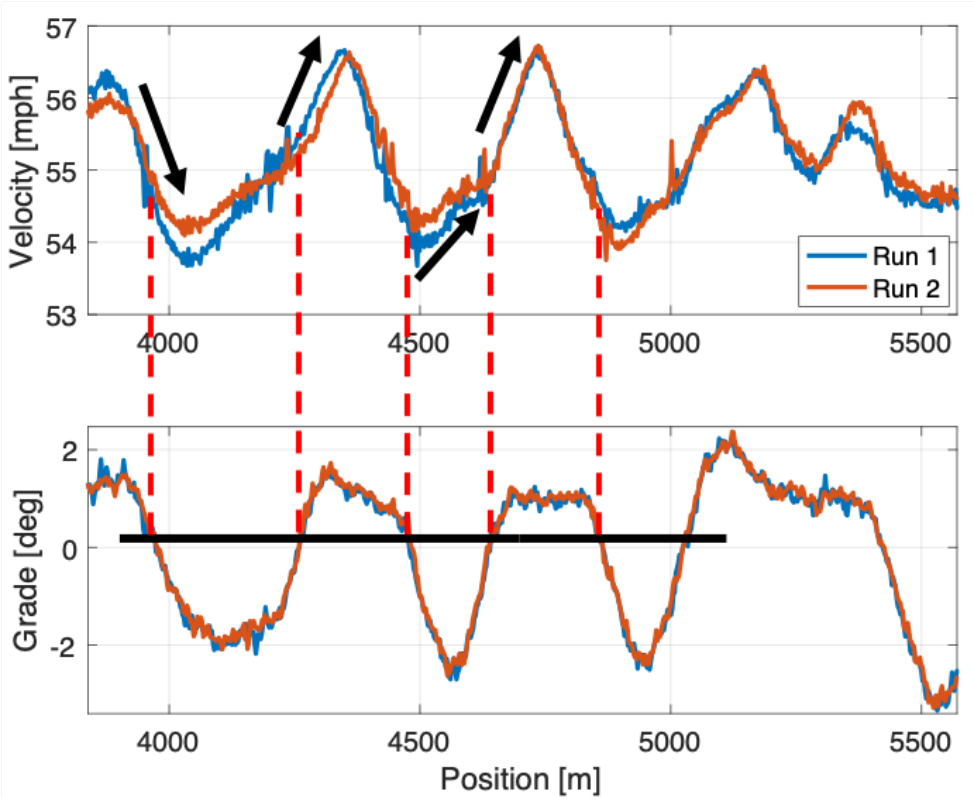

Figure 7.5: Blown-Up View of Kilometers 4-5.5 from figure 7.4

Additionally, Figure 7.6 presents the input data from the same section as Figure 7.5. This plot highlights some of the the downfalls from an energy inefficient standpoint to velocity control. Because of the increase in power needed to climb hills, downshifts are needed to increase engine RPM. Often on uphill segments the controller is commanding peak power from the engine and it can be seen that the engine fuel-rate is pinned at its upper limit.

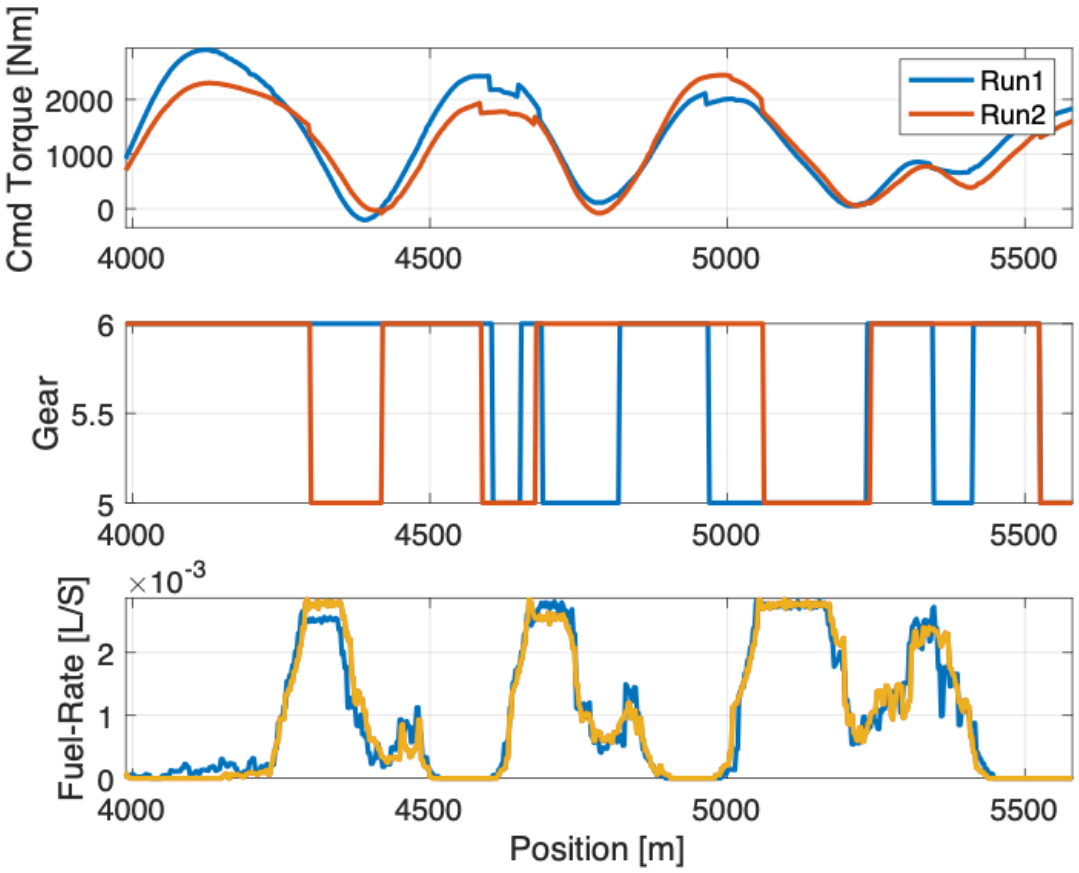

Figure 7.6: Commanded Torque by Cruise-Control System

Moving into the analysis of the eco-cruise behavior, data is provided for two runs of eco-cruise over the entirety of the test route. Figure 7.7 is markedly different than the velocity profile presented previously in Figure 7.4. Not only is the overall velocity variance higher in the eco-cruise scenario, but the velocity varies more gradually in time. The smoothness of the velocity profile alone is a good indicator of performance because a smaller acceleration is needed to maintain that velocity profile.

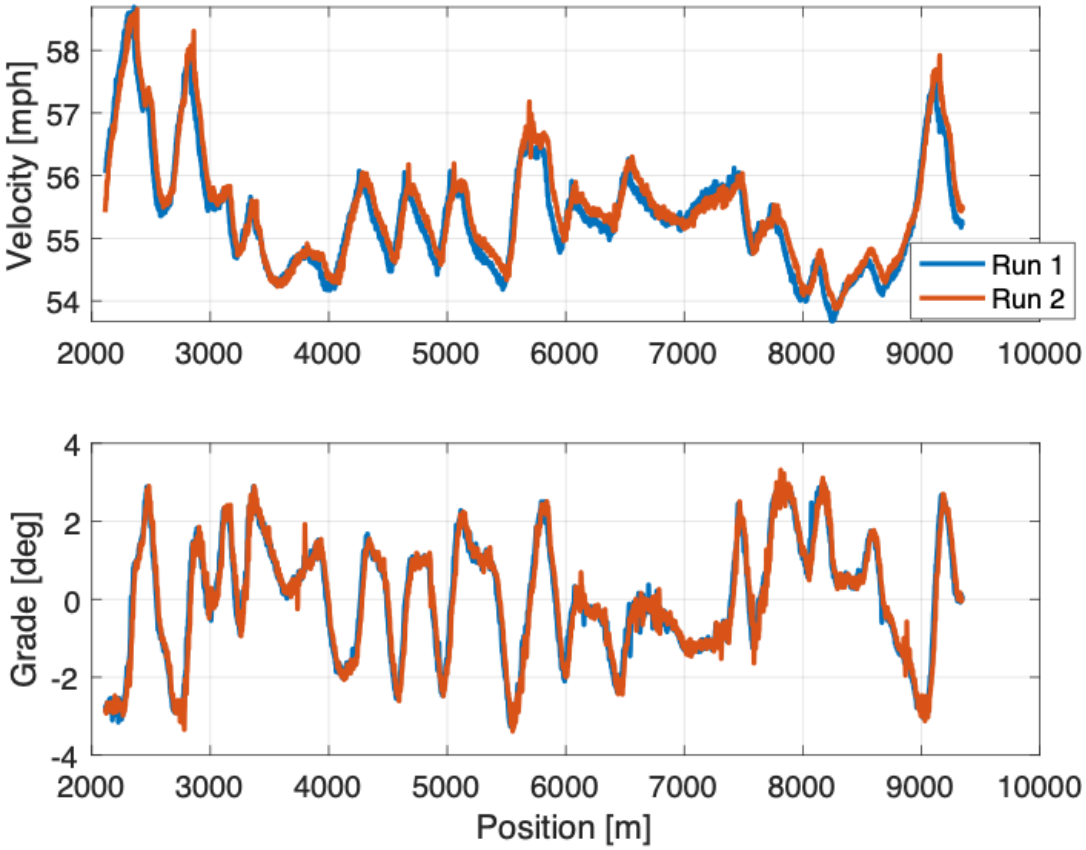

Figure 7.7: Velocity Profile of Eco-Cruise Experiments

To take a more in depth look at how exactly the eco-cruise strategy differs from the cruise control strategy, Figure 7.8 presents an exploded view of the same section of road from figure 7.5. In contrast to the cruise-control method which would accelerate uphill and brake on the downhills the eco-cruise method takes advantage of the grade to assist in efficient velocity regulation. By allowing the vehicle to accelerate on downhill segments and slow down on the uphill segments, the truck is able to retain more of its energy and requires less fuel consumption to add energy back into the system.

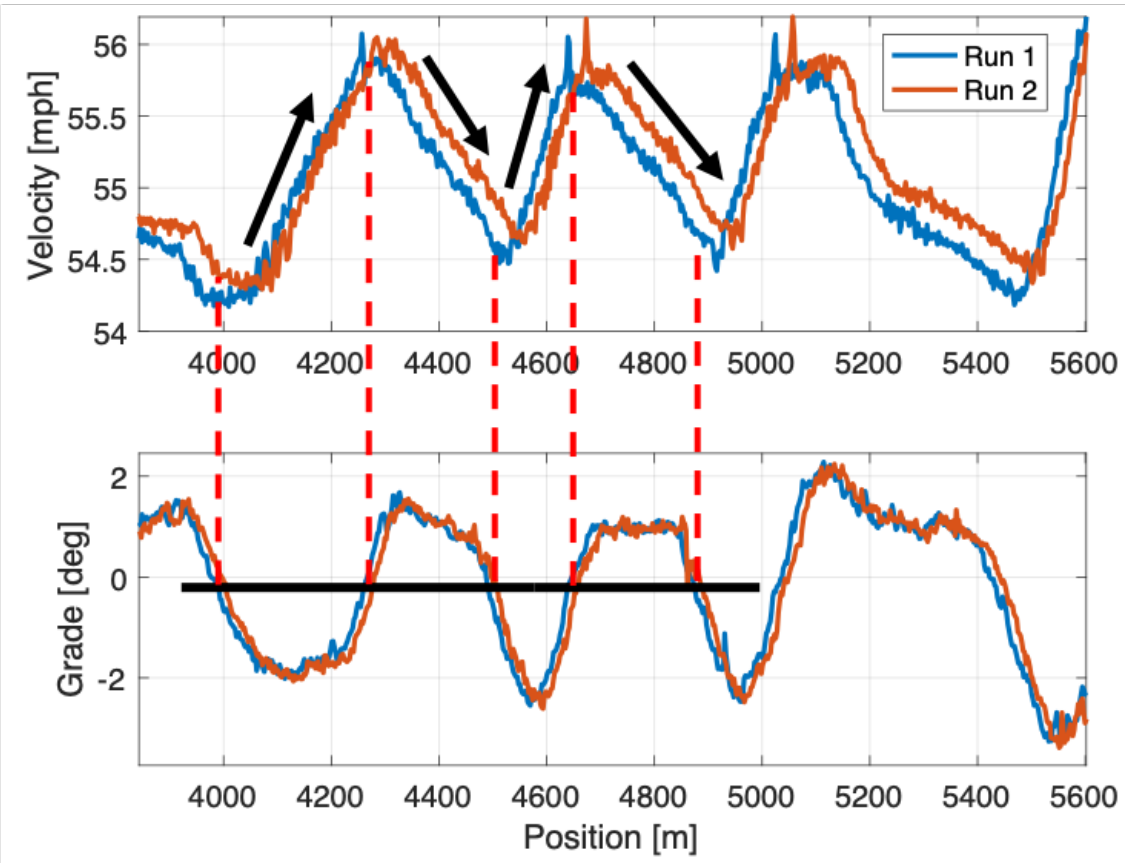

Figure 7.8: Blown-Up View of Kilometers 4-5.5 from figure 7.7

Figure 7.9 provides additional insight into the gained efficiency of the eco-cruise system. Recall from Figure 7.6 that the cruise-control system required several downshifts and a high amount of torque to climb the hills. In contrast, the eco-cruise system the system never comes close to saturating the engine which occurs at 2300Nm, doesn't need to downshift a single time and as a result, never maxes out the fuel-rate.

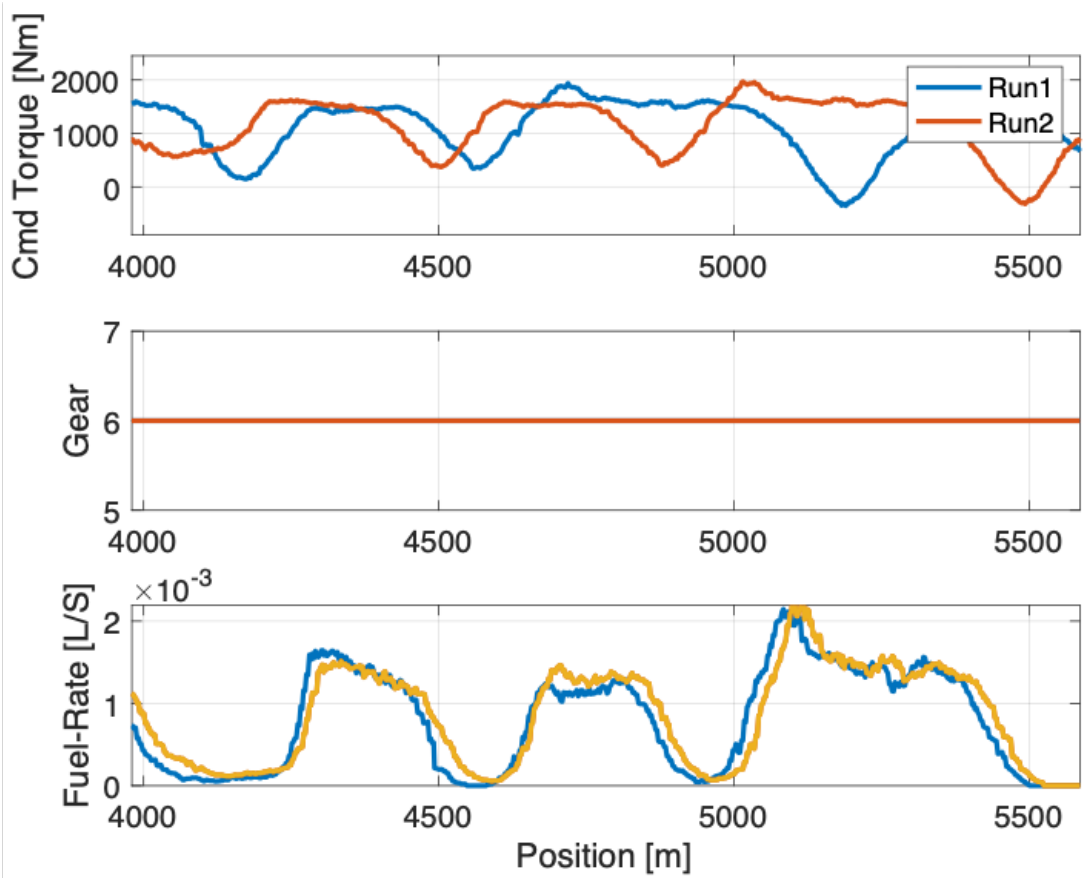

Figure 7.9: Commanded Torque by Eco-Cruise System

As already mentioned, downshifting is usually a sign that the controller is requesting high levels of engine power. By downshifting and increasing engine RPM an engine can indeed increase its power output. As a final point of comparison between the power/torque demands from the two systems, Figure 7.10 presents the average number of shift by each test configuration for the lead vehicle. Using eco-cruise the number of shifts were reduced by approximately 62%.

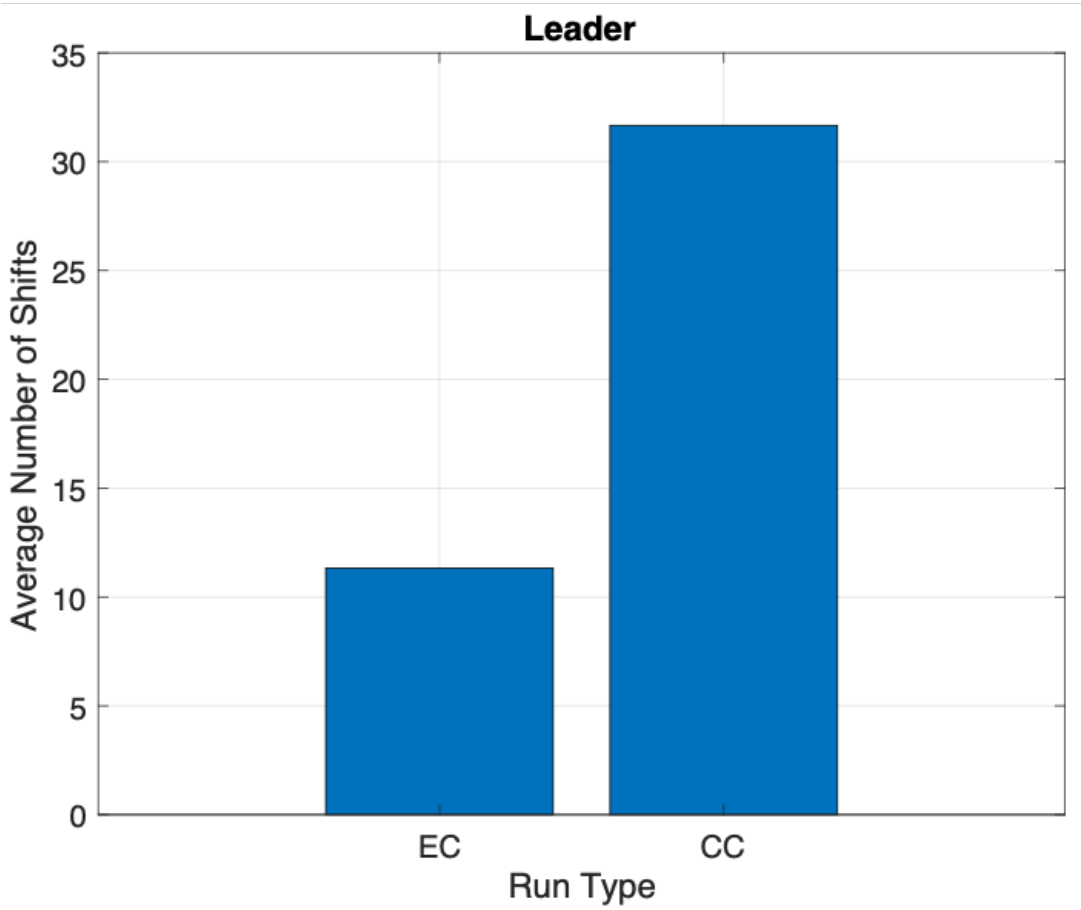

Figure 7.10: Average Shifts Per Test

7.5.2 Optimal-Following Results

A similar analysis to the one performed for the eco-cruise system was also carried out for the optimal-follower results. Figure 7.11 presents the optimal-following fuel test results. Before comparing the optimal-follower scenario to the fixed headway strategy it is worth noting that as expected, the ec-fx combination was more fuel efficient than the cc-fx combination. Because the lead vehicle had smaller acceleration magnitudes and less power demand on the engine, the following vehicle necessarily had a lower overall power demand as well resulting in added fuel savings.

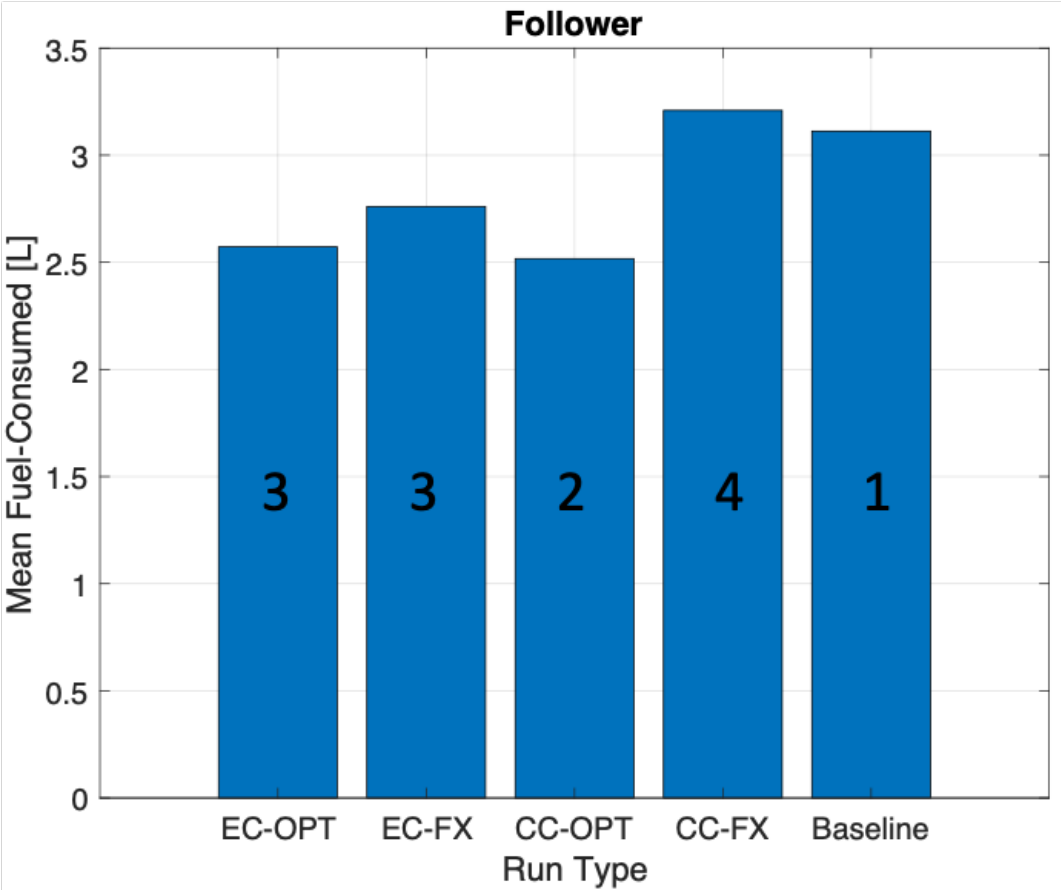

Figure 7.11: Optimal Follower Fuel Results

The main benefit of classical platooning methods comes from their ability to regulate a vehicle's headway so that it can consistently stay inside areas of high aerodynamic drag reduction. Therefore it is important that the the fixed-headway (H_∞) controller is able to regulate the headway effectively. Figure 7.12 shows that even over a section of rolling hills the headway controller is able to remain approximately within $\pm$ 4 meters of the intended reference headway. On flat terrain this would be good enough to expect roughly 7% fuel saving relative to solo driving with cruise-control [11].

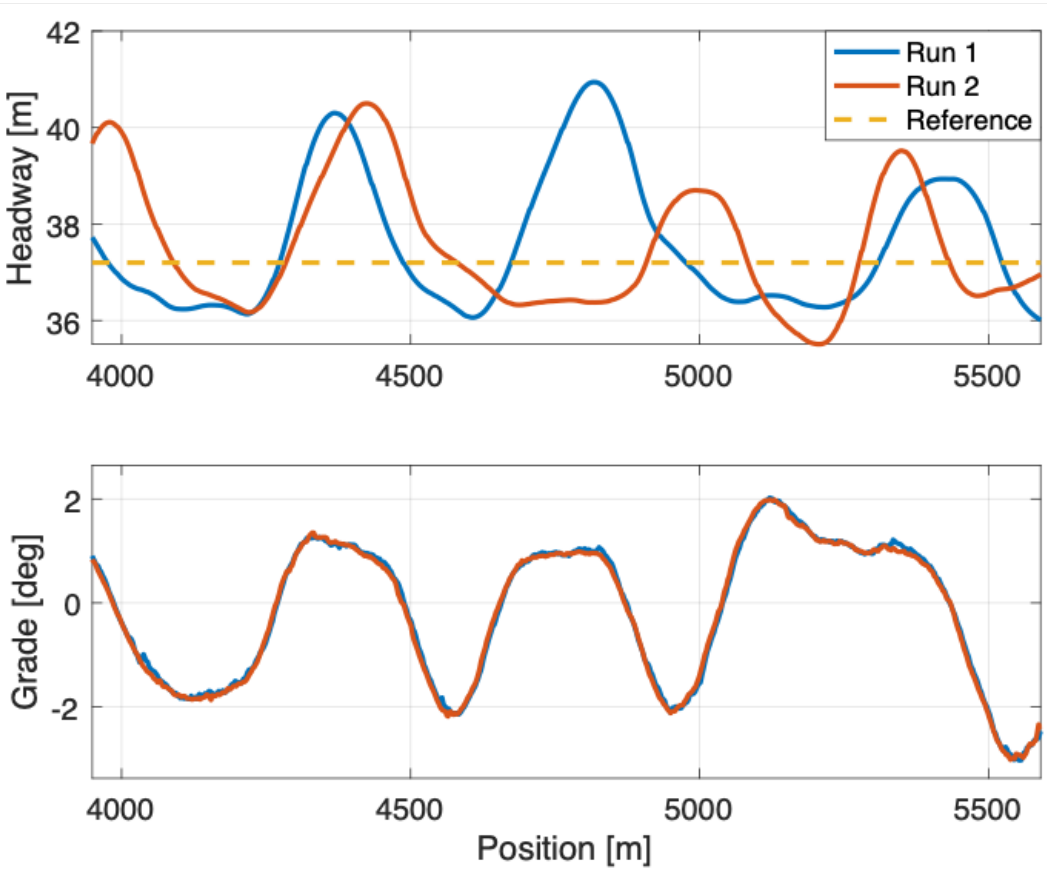

Figure 7.12: Fixed Headway Controller Performance in CC-FX Configuration

Unfortunately because the system was not on flat terrain the system is impacted by some energy inefficient moments. Figure 7.13 presents information regarding the commanded torque from the controller over the same terrain as the previous figure. Any time the torque value dips into the red area of the plot the vehicle is wasting energy. Even worse in this scenario is that the braking tends to occur on this plot during the transition from downhill to uphill. This means that the controller must command a higher torque to input energy back into the system to maintain a desired headway. This plot displays the non-saturated engine torque command as well, revealing the true magnitude of torque the controller deems necessary to maintain the given headway. The engine on the M915 vehicles is only capable of producing approximately 2300Nm of torque showing that this control architecture is running into controller saturation issues.

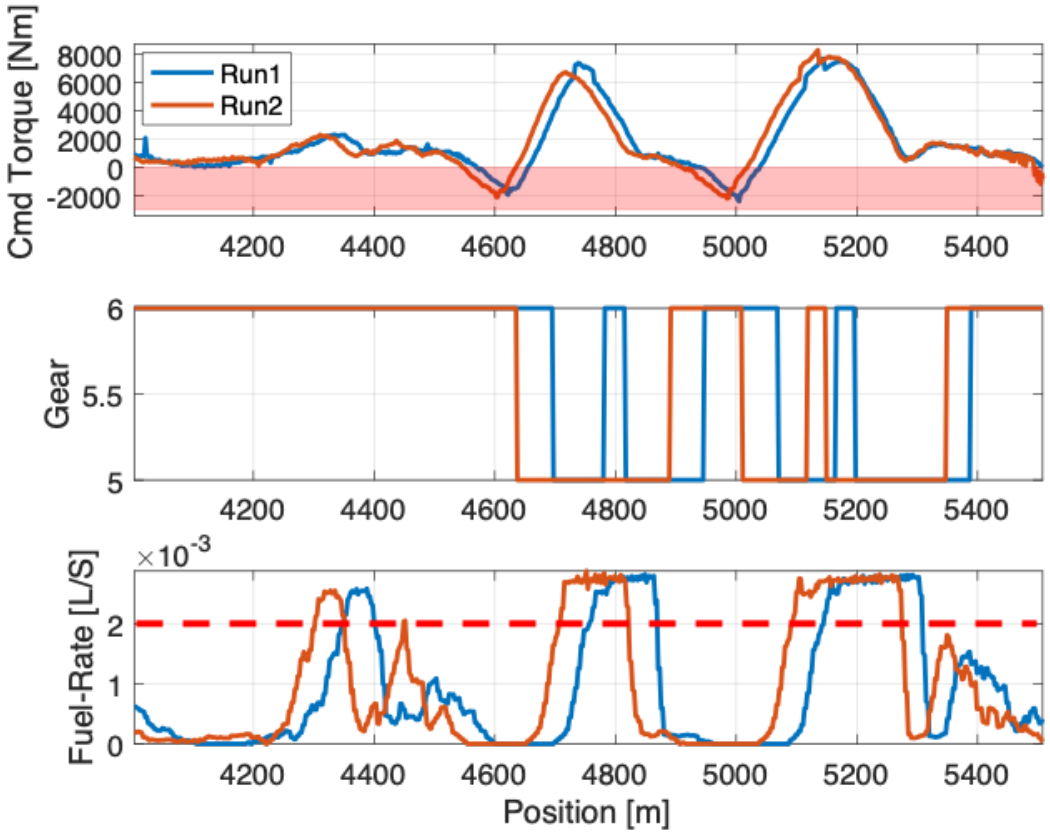

Figure 7.13: Fixed Headway Commanded Torque

It is still important for the optimal-follower platooning method to also maintain a nominal headway, but it must also balance this with a fuel-optimal driving strategy. In Figure 7.14 the headway is shown to initially close down to 30m from the desired 36.8m before encountering the rolling hills in this section. Over the next two kilometers the headway gap is allowed to fluctuate and grow by approximately 15-meters before closing down again on a steep downhill section. For the aerodynamic savings versus headway distance, the aerodynamic benefits start to level off around 35m [32]. Therefore, although the truck lost some efficiency from a reduction in the aerodynamic benefit, the reduced acceleration increases the overall energy efficiency of the vehicle.

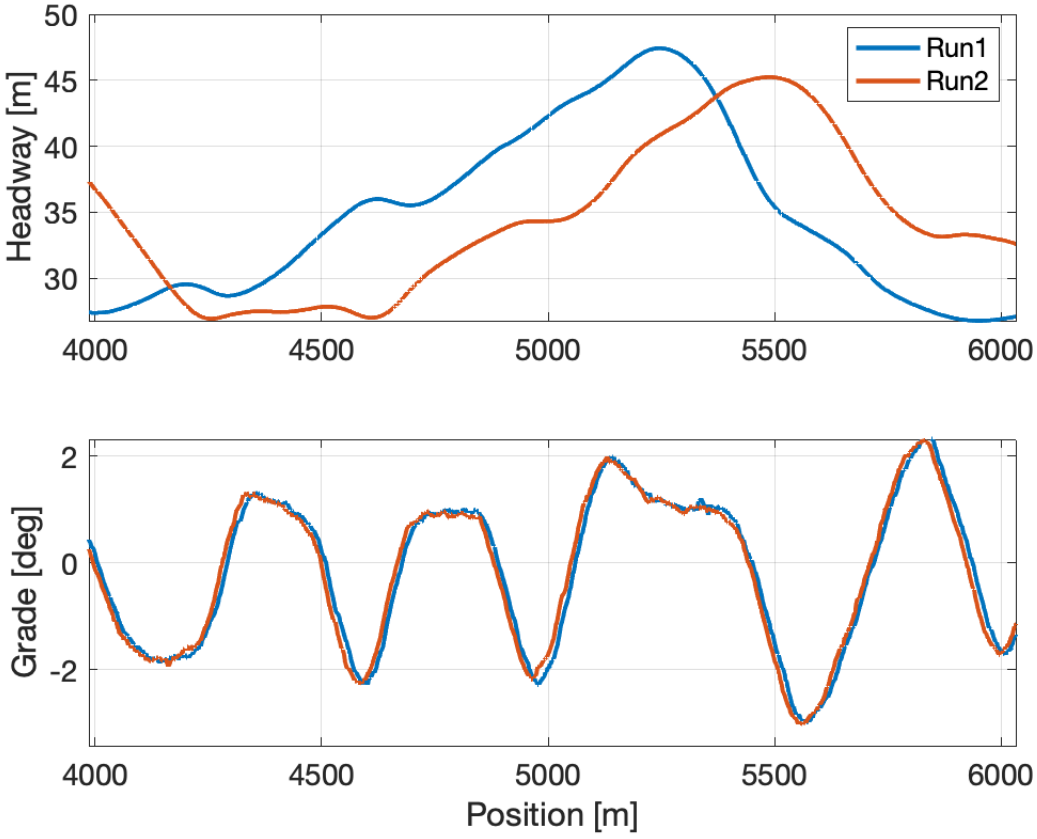

Figure 7.14: Optimal Follower Control Performance During CC-FX Platooning

To validate that the optimal-follower strategy was able to maintain the desired headway the mean headway and variance in the headway was calculate for all permissible test runs of each configuration. Table 7.4 presents these statistics and shows that the optimal strategy did indeed average the desired nominal headway of the system. The variance in the headway for the optimal strategy is larger than that of the fixed headway strategies but this is of little surprise. The goal of the optimal strategy is to balance headway with optimal driving and this is achieved by allowing for greater variation in the vehicle headway.

Table 7.4: Headway Statistics for Platooning Variations

Designation	Mean Headway [m]	Headway σ
cc fx	36.838	2.291
cc opt	35.916	8.495
ec fx	36.903	2.2604
ec hinf	36.992	1.296
ec opt	36.571	6.047

The benefit of the optimal driving strategy is also more clear when looking at the commanded torque, gear and fuel-rate. The first key benefit is that because the optimizer has an engine model built into the system, the controller can develop a strategy that avoids saturating the engine. As Figure 7.15 shows, the commanded engine torque never goes above the 2300Nm limit. Additionally because the strategy developed by the controller was not power intensive the optimal-following strategy avoided shifting gears during this segment. As a result of the low demanded engine torque and lack of gear shifts, the system does not require a high fuel-rate to bring energy back into the system. This can be better seen by referencing the red line on both figures 7.13 and 7.15. Whereas in figure 7.13 the fuel rate has sustained sections above the $2\frac{mL}{H}$ mark, the optimal following strategy never crosses that threshold a single time.

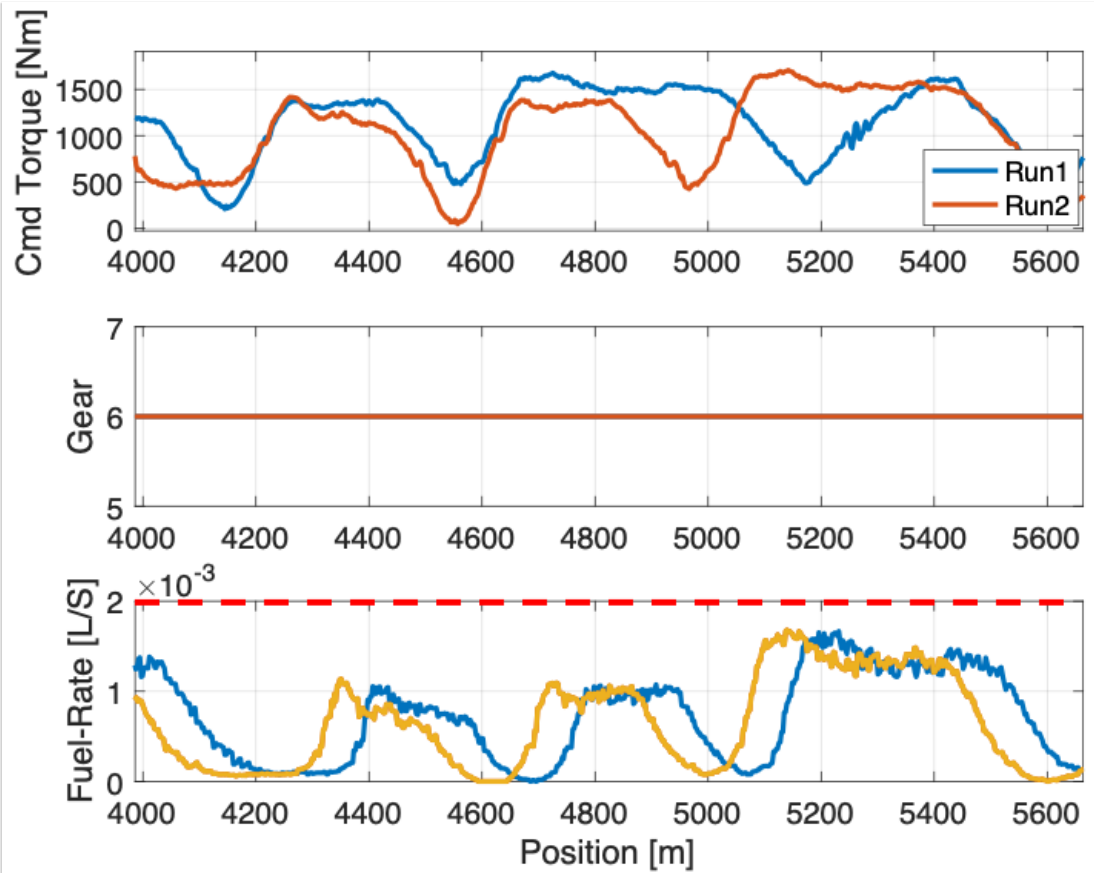

Figure 7.15: Optimal Follower Commanded Torque

Finally, as noted in previous sections, shifting can be a good indicator of how power intensive a particular control strategy is. Figure 7.16 displays the mean number of gear shifts for every tested platoon strategy. Unsurprisingly, the fixed-headway platooning methods that were relatively energy inefficient required a substantial number of gear shifts over the test terrain. When the optimal control strategy was employed, however, the number of gear shifts was drastically reduced, and when paired with eco-cruise on the lead vehicle, gear shift were completely eliminated during the test run. This also aids in eliminating any dead-time delays induced through gear shifts in the system.

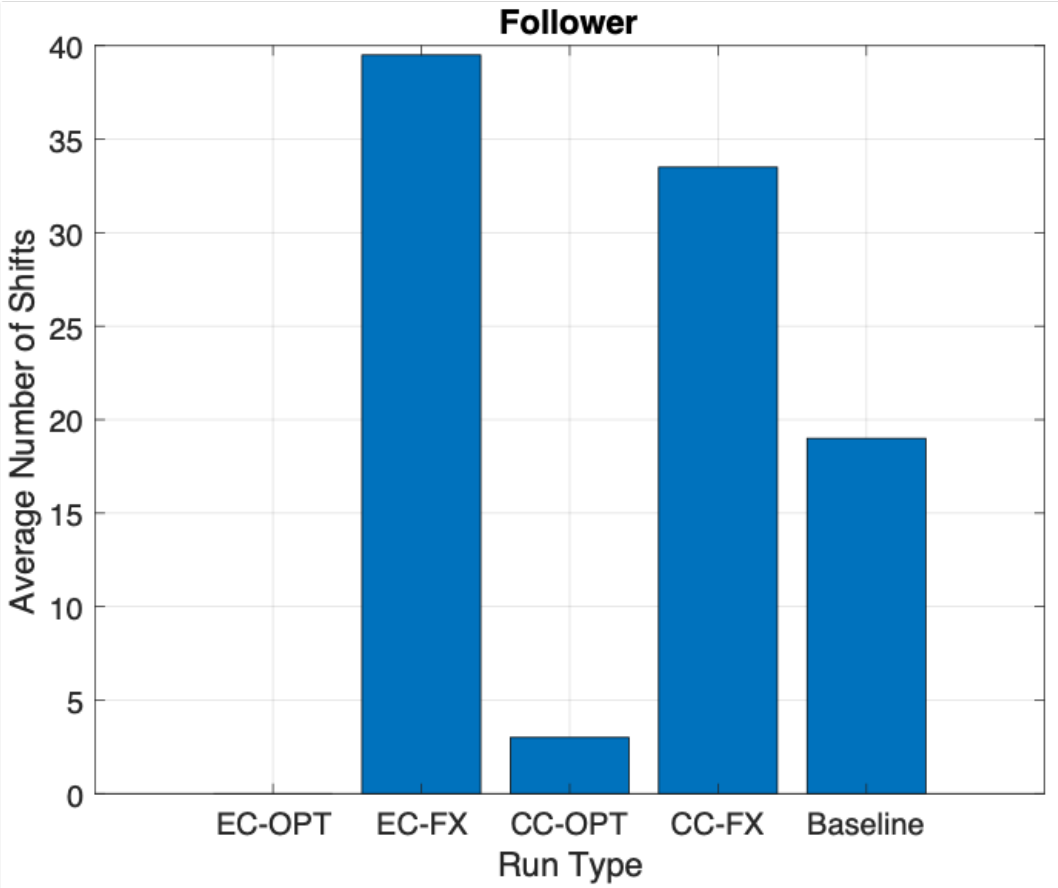

Figure 7.16: Optimal Follower Shifting Results

7.5.3 Conclusions

This chapter presented fuel results from various configurations of platooning vehicles. This testing allowed for the identification of desired cruise-control and platooning behaviors as well as behaviors that negatively impact fuel economy. Through the use of eco-cruise on the lead vehicle which takes into account upcoming terrain the lead vehicle was able to save 14.1 ±3.1% in fuel consumed over traditional cruise-control methodologies. This was in large part enabled by allowing the existing potential energy of the vehicle to transition into kinetic energy that could be carried into the next uphill segment. By preserving this energy, less had to be added in the form of consumed fuel. Additionally, the following vehicle saw fuel savings of 19.7 ±6.0%. This was achieved by not only allowing for a more efficient exchange

of the vehicle's existing potential and kinetic energy, but also by allowing the headway to fluctuate when it would be fuel-intensive to maintain a set headway.

Chapter 8

Conclusions and Future Works

8.1 Conclusions

As vehicle efficiency becomes increasingly important in today's world, practical and efficient platooning methods that can handle real-world terrain will continue to be an active area of research. This thesis introduced a distributed method of optimal control for both a leader and follower vehicle in a platoon. Prior art was investigated, and the design choices of other systems were introduced and discussed. The design and implementation of the new O.C. system was then covered. Finally the system was evaluated both in simulation and in the real world on varying grade roads such as Alabama Highway 280.

The 3-link fuel model for determining fuel-rate from vehicle wheel speed was then introduced. This 3-link mechanism was validated against measured data to validate accuracy. While the Brake Specific Fuel Consumption (BSFC) map can be hard to determine, a method for generating a fuel-rate polynomial was presented. Through analysis of multiple types of fuel-rate polynomials a polynomial with satisfactory model was picked. Finally the fuel-rate polynomials were validated against measured fuel-rate data with the linear approximation having 4.9% error over a 6.5 minute test run whereas the non-linear fuel rate only had a .9% error over the same test run.

Additionally, a new H_∞ classical-controller was designed that would guarantee string-stability over flat-terrain. This controller also accounted for delays in communication from one vehicle to the next and accounted for the vehicle spacing policy within the control architecture. While this system was proven to be string-stable on flat ground, the system still performed unfavorably on hilly terrain. The key reason for this was that the system

had no ability to mitigate actuator saturation issues, which cause very energy inefficient dynamics.

Finally, the Eco-Cruise and Optimal-Follower systems were tested on public roads. By building a terrain map, an appropriate look ahead distance for the optimizer was selected. By including an engine model in the optimizer the system was able to avoid any saturation issues. Additionally, the system was able to more efficient transfer the system from potential energy to kinetic energy. This was achieved by allowing the system to carry more speed through a downhill section without braking. This resulted in a platooning system that allowed the lead truck to see a 14% $\pm$ 3.4% fuel savings benefit. Additionally the following vehicle saw a fuel savings of 19.7% pm .0%. This proves that a platooning system that accounts for upcoming terrain is more than capable of increasing semi-truck fuel efficiency

8.2 Future Work

As with all research, at the conclusion of this project resulted in some ideas for future improvements. While several different design considerations were made, not all were able to be explored. some of these different design choices include altering an existing part of the controller to increase platoon safety, sharing additional information between vehicle, and changing test methodologies to further increase reader confidence in the presented fuel results.

The first major update would be to the PID loop that helps regulate the vehicle velocity of the O.C. system. The PID controller only regulates the vehicle velocity and has no considerations of the headway between two vehicles. By introducing an inner loop MPC controller that uses a linearized vehicle model, the inner loop could help enforce safety constraints and minimum headway constraints during periods of fast dynamics such as hard braking.

Additionally, being able to share the generated vehicle velocity profile from one vehicle to the next would be extremely advantageous. Most current systems that do this make an

implicit assumption that all vehicles in the platoon are using the same look-ahead distance and have the same prediction horizon length. To try and keep the system as generic as possible it would also be necessary to transmit the look-ahead distance associated with the velocity profile so that any vehicle can make use of it. By sharing the generated velocity profile, the following vehicle's would no longer have to make assumptions about the behavior of the lead trucks velocity. This would allow the followers to generate a safer velocity profile. By sharing the velocity profile down the line sequentially one could guarantee that there would be no collisions in the platoon.

Finally, some readers may note that the test vehicle's are older model Freightliner M915's with only a 6-speed transmission. While the main advantages of the system come from a more efficient driving method, there is indeed an increase in fuel consumption cause by the lack of gears in the class-8 vehicles used. By using a more modern test vehicle with improved aerodynamics and more gears readers can be more confident that the key benefit is indeed with the driving method and not just a function of improved aerodynamics.

Bibliography

[1] *ANNUAL VEHICLE DISTANCE TRAVELED IN MILES AND RELATED DATA - 2018(1) BY HIGHWAY CATEGORY AND VEHICLE TYPE*. [Online]. Available: https://www.fhwa.dot.gov/policyinformation/statistics/2018/pdf/vm1.pdf (visited on 06/26/2021).

[2] M. P. Lammert, B. McAuliffe, P. Smith, A. Raeesi, M. Hoffman, and D. Bevly, "Impact of lateral alignment on the energy savings of a truck platoon," presented at the WCX SAE World Congress Experience, Apr. 14, 2020, pp. 2020–01–0594. DOI: 10.4271/2020-01-0594. [Online]. Available: https://www.sae.org/content/2020-01-0594/ (visited on 04/23/2021).

[3] M. P. Lammert, A. Duran, J. Diez, K. Burton, and A. Nicholson, "Effect of platooning on fuel consumption of class 8 vehicles over a range of speeds, following distances, and mass," *SAE Int. J. Commer. Veh.*, vol. 7, no. 2, p. 14, 2014.

[4] S. S. Stankovic, M. J. Stanojevic, and D. D. Siljak, "Decentralized overlapping control of a platoon of vehicles," *IEEE TRANSACTIONS ON CONTROL SYSTEMS TECHNOLOGY*, vol. 8, no. 5, p. 17, 2000.

[5] A. Alam, "Fuel-ecient distributed control for heavy duty vehicle platooning," p. 109,

[6] J. Ploeg, N. van de Wouw, and H. Nijmeijer, "Lp string stability of cascaded systems: Application to vehicle platooning," *IEEE Transactions on Control Systems Technology*, vol. 22, no. 2, pp. 786–793, Mar. 2014, ISSN: 1063-6536, 1558-0865. DOI: 10.1109/TCST.2013.2258346. [Online]. Available: http://ieeexplore.ieee.org/document/6515636/ (visited on 07/08/2020).

[7] J. Ploeg, B. T. M. Scheepers, E. van Nunen, N. van de Wouw, and H. Nijmeijer, "Design and experimental evaluation of cooperative adaptive cruise control," p. 6,

[8] M. Roeth, S. Road, and F. Wayne, "Peloton technology platooning test nov 2013," p. 11, 2013. [Online]. Available: https://www.itskrs.its.dot.gov/its/benecost.nsf/ID/b34bdbc4e55a105c852580ea004f739f.

[9] G. Apperson, "Design and evaluation of cooperative adaptive cruise control system for heavy freight vehicles," PhD thesis, Dec. 14, 2019. [Online]. Available: https://etd.auburn.edu/handle/10415/7069?show=full.

[10] D. Bevly, C. Murray, A. Lim, and a. et al, *Heavy truck cooperative adaptive cruise control: Evaluation, testing and stakeholder engagement for near term deployment: Phase one final report*, May 27, 2015. [Online]. Available: https://truckingresearch.org/2015/05/27/4410/.

[11] B. McAuliffe, M. Lammert, X.-Y. Lu, S. Shladover, M.-D. Surcel, and A. Kailas, "Influences on energy savings of heavy trucks using cooperative adaptive cruise control," presented at the WCX World Congress Experience, Apr. 3, 2018, pp. 2018–01–1181. DOI: 10.4271/2018-01-1181. [Online]. Available: https://www.sae.org/content/2018-01-1181/ (visited on 07/14/2021).

[12] H. Xing, J. Ploeg, and H. Nijmeijer, "Padé approximation of delays in cooperative ACC based on string stability requirements," *IEEE Transactions on Intelligent Vehicles*, vol. 1, no. 3, pp. 277–286, Sep. 2016, ISSN: 2379-8904, 2379-8858. DOI: 10.1109/TIV.2017.2662482. [Online]. Available: http://ieeexplore.ieee.org/document/7839205/ (visited on 05/13/2020).

[13] I. Ibitayo, "Enhanced class-8 truck platooning via simultaneous shifting and model predictive control," PhD thesis, Purdue University, Aug. 2019.

[14] W. Huang, "Wei_huang_dissertation.pdf," PhD thesis, Auburn University, Aug. 9, 2010. [Online]. Available: https://etd.auburn.edu/handle/10415/2252.

[15] A. Alam, "Fuel-efficient heavy-duty vehicle platooning.pdf," PhD thesis, KTH Royal Institute of Technology, Jun. 13, 2014. [Online]. Available: http://kth.diva-portal.org/smash/record.jsf?pid=diva2%3A719084&dswid=6614.

[16] V. Turri, B. Besselink, and K. H. Johansson, "Cooperative look-ahead control for fuel-efficient and safe heavy-duty vehicle platooning," *IEEE Transactions on Control Systems Technology*, vol. 25, no. 1, pp. 12–28, Jan. 2017, ISSN: 1063-6536, 1558-0865. DOI: 10.1109/TCST.2016.2542044. [Online]. Available: http://ieeexplore.ieee.org/document/7445860/ (visited on 04/19/2021).

[17] J. W. Ward, E. M. Stegner, M. A. Hoffman, and D. M. Bevly, "A method of optimal control for class 8 vehicle platoons over hilly terrain," *Journal of Dynamic Systems, Measurement, and Control*, vol. 144, no. 1, p. 011 108, Jan. 1, 2022, ISSN: 0022-0434, 1528-9028. DOI: 10.1115/1.4053087. [Online]. Available: https://asmedigitalcollection.asme.org/dynamicsystems/article/144/1/011108/1128821/A-Method-of-Optimal-Control-for-Class-8-Vehicle (visited on 08/09/2022).

[18] D. Hall and J. Moreland, "Fundamentals_of_rolling_resist.pdf," *Rubber Chemistry and Technology*, vol. 74, no. 3, pp. 525–539, Jul. 2001.

[19] P. Smith, "Evaluation of platooning efficiency for heavy duty trucks using cooperative adaptive cruise control," PhD thesis, Auburn University, May 20, 2020. [Online]. Available: https://etd.auburn.edu/handle/10415/7241.

[20] E. Shi, T. M. Gasser, A. Seeck, and R. Auerswald, "The principles of operation framework: A comprehensive classification concept for automated driving functions," *SAE International Journal of Connected and Automated Vehicles*, vol. 3, no. 1, pp. 12–03–01–0003, Feb. 18, 2020, ISSN: 2574-075X. DOI: 10.4271/12-03-01-0003. [Online]. Available: https://www.sae.org/content/12-03-01-0003/ (visited on 07/16/2021).

[21] M. Quigley, B. Gerkey, K. Conley, J. Faust, T. Foote, J. Leibs, E. Berger, R. Wheeler, and A. Ng, "ROS: An open-source robot operating system," p. 6,

[22] P. Groves, *Principles of GNSS, Inertial, and Multi-sensor Integrated Navigation Systems*. Artech House, Apr. 27, 2008, ISBN: 978-1-60807-005-3. (visited on 08/09/2022).

[23] P. Smith, J. Ward, J. Pierce, D. Bevly, and R. Daily, "Experimental results and analysis of a longitudinal controlled cooperative adaptive cruise control (CACC) truck platoon," presented at the Dynamic Systems and Controls Conference, 2019, p. 9.

[24] P. Apkarian and D. Noll, "Nonsmooth h synthesis," *IEEE Transactions on Automatic Control*, vol. 51, no. 1, pp. 71–86, Jan. 2006, ISSN: 0018-9286, 1558-2523. DOI: 10.1109/TAC.2005.860290. [Online]. Available: http://ieeexplore.ieee.org/document/1576856/ (visited on 07/22/2021).

[25] P. Apkarian and D. Noll, "The h control problem is solved," p. 27,

[26] *A Policy on Geometric Design of Highways and Streets*. American Association of State Highway and Transportation Officials, 2001, 905 pp., ISBN: 1-56051-156-7.

[27] E. Wood, A. Duran, E. Burton, J. Gonder, and K. Kelly, "EPA GHG certification of medium- and heavy-duty vehicles: Development of road grade profiles representative of US controlled access highways," *Renewable Energy*, p. 79, 2015.

[28] A. Alam and V. Turri, "Heavy-duty vehicle platooning for sustainable freight transportation: A cooperative method to enhance safety and efficiency," *IEEE Control Systems*, vol. 35, no. 6, pp. 34–56, Dec. 2015, ISSN: 1066-033X, 1941-000X. DOI: 10.1109/MCS.2015.2471046. [Online]. Available: https://ieeexplore.ieee.org/document/7286902/ (visited on 07/26/2021).

[29] R. Brothers, "A COMPARISON OF VEHICLE HANDLING FIDELITY BETWEEN THE GAZEBO AND ANVEL SIMULATORS," p. 13, 2018.

[30] J.-H. Lo, S. Eye, S. M. Rohde, and M. M. Rohde, "2016 NDIA GROUND VEHICLE SYSTEMS ENGINEERING AND TECHNOLOGY SYMPOSIUM AUTONOMOUS GROUND SYSTEMS (AGS) TECHNICAL SESSION AUGUST 2-4, 2016 - NOVI, MICHIGAN," p. 10, 2016.

[31] J. SAE, *Fuel consumption test procedure - type II*, 2020.

[32] B. McAuliffe, A. Raeesi, M. Lammert, P. Smith, M. Hoffman, and D. Bevly, "Impact of mixed traffic on the energy savings of a truck platoon," presented at the WCX SAE World Congress Experience, Apr. 14, 2020, pp. 2020–01–0679. DOI: 10.4271/2020-01-0679. [Online]. Available: https://www.sae.org/content/2020-01-0679/ (visited on 07/25/2021).

Appendices

Appendix A

Exact Fuel Test Measurements

Table A.1: Raw Fuel Results for the Lead Vehicle

Eastbound	Iteration	Test L/hr	Control L/hr	T/C
cc	1	39.556	32.819	1.205
cc fx	1	39.836	33.664	1.183
cc fx	2	40.417	33.740	1.198
cc fx	3	40.893	33.509	1.220
cc opt	1	39.496	33.184	1.190
cc opt	2	40.275	34.108	1.181
cc hinf	1	39.446	32.736	1.205
ec fx	1	33.988	32.744	1.038
ec hinf	1	34.016	34.000	1.000
ec opt	1	34.908	34.201	1.021
ec opt	2	34.679	33.482	1.036
ec opt	3	34.723	33.054	1.050

Table A.2: Raw Fuel Results for the Follow Vehicle

Eastbound	Iteration	Test L/hr	Control L/hr	T/C
cc	1	34.298	32.819	1.045
cc fx	1	35.172	33.664	1.045
cc fx	2	35.585	33.740	1.055
cc fx	3	36.498	33.509	1.089
cc opt	1	28.107	34.000	0.827
cc opt	2	27.640	33.184	0.833
cc hinf	1	33.977	32.736	1.038
ec fx	1	30.315	32.744	0.926
ec hinf	1	32.221	33.144	0.972
ec hinf	2	31.009	34.475	0.899
ec opt	1	28.428	34.201	0.831
ec opt	2	27.651	32.762	0.844
ec opt	3	29.452		
ec opt	4	28.555	33.054	0.864

Appendix B

SAE-J1321 Fuel Results Calculation Worksheets

B.1 Eco-Cruise

Table B.1: Eco-Cruise T/C Ratio Calculator

Baseline Segment		Date:	
Consumed fuel (kg or lb. or gal.)			
Run	Test Vehicle	Control Vehicle	T/C
1	3.56	3.02	1.1789
2	3.57	3.07	1.1638
3	3.60	3.11	1.1578
4			

Cruise Control

Test Segment		Date:	
Consumed fuel (kg or lb. or gal.)			
Run	Test Vehicle	Control Vehicle	T/C
1	3.15	3.17	0.9941
2	3.12	3.06	1.0211
3	3.09	3.02	1.0225
4	3.05	3.14	0.9711

Eco-Cruise

Table B.2: Eco-Cruise T-Test

T-Test with Equal Variances (2-tailed)	
Pooled St dev	0.02019
t-crit	2.571
t-stat	10.672
Is Fuel Economy Improved?	YES
P-value	0.0001250
lower CI bound	0.12495
upper CI bound	0.20424

Table B.3: Eco-Cruise Fuel Savings

Test Result			
	Nominal	Confidence Interval	
Fuel Savings	14.1%	±	3.4%

B.2 Optimal-Following

Table B.4: Optimal-Following T/C Ratio Calculator

Baseline Segment		Date:	
Consumed fuel (kg or lb. or gal.)			
Run	Test Vehicle	Control Vehicle	T/C
1	3.20	3.07	1.0423
2	3.24	3.13	1.0342
3	3.33	3.13	1.0629

Fixed Headway

Test Segment		Date:	
Consumed fuel (kg or lb. or gal.)			
Run	Test Vehicle	Control Vehicle	T/C
1	2.57	3.17	0.8107
2	2.66	3.02	0.8808
3	2.54	3.06	0.8301

Optimal following

Table B.5: Optimal-Following T-Test

T-Test with Equal Variances (2-tailed)	
Pooled St dev	0.02765
t-crit	2.776
t-stat	9.123
Is Fuel Economy Improved?	YES
P-value	0.0008009
lower CI bound	0.14326
upper CI bound	0.26860

Table B.6: Optimal-Following Fuel Savings

Test Result			
	Nominal	Confidence Interval	
Fuel Savings	19.7%	±	6.0%